SUPPLEMENTAL APPENDIX EXTENDED METHODS

Expression and purification of wild-type, mutant and truncated Pus7 proteins.

Saccharomyces cerevisiae wild-type and truncated ($Pus7_{\Delta N34C9}$, $Pus7_{\Delta IDI}$) Pus7 protein encoding DNA-sequences were ordered from GeneArt. Ligation independent cloning was used to incorporate these sequences into a pMCSG7 vector containing an N-terminal His_6-tag and TEV cleavage site. Single and double mutants were incorporated into the Pus7 sequence by QuikChange® site-directed mutagenesis (Stratagene) using appropriate primers (IDT) (SI Methods). Sequences were confirmed by Sanger DNA sequencing (UMich sequencing core). All proteins were expressed in BL21(DE3)-P-LysS *E. coli* cells grown in 1L Terrific Broth, 100 µg/mL ampicillin at 37°C and 250 RPM. Protein expression was induced by the addition of isopropyl β-D-1-thiogalactopyranoside (IPTG) to a final concentration of 0.15 mM when cells reached OD_{600} of ~0.6. Following induction, cells were grown for 18 hours at 20°C and harvested by centrifugation at 5,000 RPM for 30 minutes. Pus7 proteins were purified on a Ni^{2+} Hi-Trap column (GE healthcare), the His-tag was removed by TEV protease treatment followed by a second Ni^{2+} Hi-Trap column. The protein was further purified by anion exchange chromatography on a 5 mL Resource™ Q column (GE Healthcare), and size exclusion chromatography using a Superdex 200 column (GE Healthcare). Purified protein was either concentrated and stored at -80° C or used immediately for crystallization.

Selenomethionine Expression

pMCSG7-yPus7 was expressed in BL21(DE3) cells grown in Terrific Broth media (4% glycerol), 100 µg/mL ampicillin at 37°C overnight. The cells were pelleted resuspended in 1.1L of selenomethionine minimal media, supplemented with 50 µg/mL L-selenomethionine, and 100 mL of freshly prepared, and sterile filtered nutrient solution 20% (w/v) glucose, 0.3% (w/v) $MgSO_4$, 0.1mg/mL $Fe(II)(SO_4)_3$, 0.1 mg/mL Thiamine, adjust to pH 7.4, sterile. The cells were then grown at 37°C and 250 RPM until OD_{600} of 0.6. The cells were induced with IPTG to a final concentration of 0.2 mM and grown for 18 hours at 20°C before harvesting by centrifugation.

Crystallization

Unlabeled and SeMet derivatized Pus7 was concentrated 10 mg/mL in 50 mM TRIS, pH 7.5, 50 mM NaCl, 1 mM tris(2-carboxyethyl)phosphine (TCEP). Crystals of Pus7 were obtained by the sitting-drop vapor-diffusion method at 20°C by mixing 0.5uL of protein solution (10mg/mL) with 0.5uL of the reservoir solution which contained 2 M ammonium sulfate, 10 mM nickel (II) chloride, 100 mM TRIS pH 8.5. The crystals were then cryoprotected in a solution of 15% glycerol, 1.7 M ammonium sulfate, 0.85 mM nickel (II) chloride, 85 mM TRIS pH 8.5 before being flash cooled in liquid-nitrogen.

Crystal data processing

Diffraction data were collected at 100 K and at the Se edge on LS-CAT 21-ID-D at Advanced Photon Source, Argonne National Laboratory using a DECTRIS EIGER 9M. Three data sets were collected from two crystals, and all were separately processed with XDS to 3.2 Å resolution were Friedel pairs were treated as equal. Reflections from a total of 1500 selected frames (first 500 from 2 datasets and first 400 from the third) were merged and scaled with Aimless (cite) and the

resulting reflection file was used for subsequent refinements of our Pus7 model. The data were indexed to space group C222 (unit-cell parameters *a* = 117.9, *b* = 171.8, *c* = 105.3 Å) with 1 molecule in the asymmetric unit (Matthew's coefficient V_M = 3.46 Å^3 Da^{-1}, 64.5% solvent content). 500 frames from a single data set were processed anomalous (Friedel pairs were not treated as equal) with XDS to 3.2 Å and the resulting reflection file was used for the SAD phasing.

Crystal structure solution

Initial structure solutions were obtained by molecular replacement using the human Pus7 (PDB:5KKP) as a search model and initial phases were calculated using Phaser (1). However, we were unable to obtain a structure solution for insertion domain one, which necessitated the growth of Se-Met Pus7 crystals. AutoSol (2) was used to identify selenium sites and calculate density-modified 3.3 Å experimental maps based on a single-wavelength single-wavelength anomalous dispersion (SAD) data set from SeMet Pus7 (the experimentally determined SeMet f' and f" values that were used were -7.4 and 5.0 respectively). Specifically, 16 selenium sites were located and used for SAD phasing, using phenix.hyss. Subsequently, Phaser was used to calculate the experimental phases, followed by density modification with RESOLVE (figure of merit 0.36 before and 0.78 after density modification). The experimental density map showed clear features of the protein backbone and well-defined side chains. RESOLVE traced and automatically built 389 residues and their side chains in the experimental electron density. The final experimental model was in really good agreement with our original MR derived model but also provided us with a partial model of ID-1. The partial model of ID-1 included residues 129 to 148, a region of ID-1 that packs against the core of an adjacent monomer and includes the only SeMet present in ID1. The electron density corresponding to the insertion domain is overall poor and of rather low resolution, as also reflected in the very high average B-factors (165.02) as compared to the average B-factors (117.44) for the rest of the protein (Figure S2E). Ultimately, using SAD phasing, in combination with our MR model, we were able to obtain a structure solution for the insertion domain, completing our structure model. An overlay of the final Pus7 model with all 16 experimentally determined selenium heavy atoms is shown in Fig. S2. The structural model was refined with REFMAC5 as part of the CCP4I2 package (3) using isotropic individual *B*-factors with maximum-likelihood targets where the Babinet model for bulk-solvent scaling was utilized. Refinement was followed by model building and modification with Coot (4). We performed several iterative rounds of refinement followed by model building and modification. All crystallographic information as well as refinement statistics are provided in Table 1. The geometric quality of the model and its agreement with the structure factors were assessed with MolProbity (5). Figures displaying crystal structures were generated by PyMOL(6).

Preparation of 5'-fluorescein labeled RNA substrates.

RNA was prepared via *in vitro* transcription from DNA oligonucleotide templates ordered from Integrated DNA Technologies (IDT) and transcribed by recombinant T7 RNA polymerase (7). Transcription reactions were carried out in 50 mM Tris-HCl pH 8.0, 4 mM $MgCl_2$, 1 mM spermidine, 5 mM DTT, 4 mM ATP, 4 mM CTP, 4 mM UTP, 1 mM GTP, 4 mM guanosine-5'-O-monophosphorothiolate (GMPS), 350 µg/mL purified T7 RNA polymerase, 12.5 µM purified DNA template containing T7 promoter and 4 U/µl SUPERaseIn. After stopping the transcription by the addition of 50 mM EDTA and 500 mM NaCl, the RNA was washed with degassed TE pH 7.2 three

times using Amicon spin column (10 kDa MWCO). The washed RNA (~250 µl) was incubated with 20 µl 45 mM fluorescein overnight at 37°C to label the 5'end. All following steps were carried out in the dark. The reaction was stopped by addition of an equal volume of 2X loading dye (0.05% Bromophenol Blue, 0.05% Xylene Cyanol dye, 50% m/v urea, 0.1 M EDTA) and run on a 12% urea-polyacrylamide gel. The RNA was eluted via crush-and-soak method into buffer (TE, 0.1% SDS, and 0.5 M NaCl) overnight at 4°C. The elution products were subsequently filtered, washed, and concentrated using degassed TE and an Amicon spin column (10 kDa MWCO). The RNA was then ethanol precipitated at -20°C for 12 hours. The resulting pellet was resuspended in 20 µl of RNase free H_2O. The concentration of the total and labeled RNA were measured photometrically using A260 and A494 respectively, using a Nanodrop spectrophotometer. Select Fl-labeled substrates were also purchased from Dharmacon.

Electrophoretic mobility shift assays (EMSAs)

For gel-shift assays, serially diluted protein (0-2000 µM) was incubated with 10 nM of 5'-fluorescein labeled RNA in 10 µL reaction volumes for ≥ 5 min at 25°C in a binding buffer containing 100 mM NH_4OAc, 100 mM Tris, pH 8.0, 5 mM $MgCl_2$, 2 mM DTT, and 6% (w/v) sucrose. An aliquot of each reaction (5 µL) was loaded on a preequilibrated, native 6% polyacrylamide (37.5:1) gel in 1xTBE. Gels were electrophoresed at 30V for ~4h at 4°C. When fluorescently labeled RNA substrates were used, electrophoresis was performed in the dark. Gels were then rinsed in 1xTBE and imaged on an Amersham Typhoon Biomolecular Imager (GE Healthcare). If unlabeled RNA was used, the gel was stained with SYBR® Gold Nucleic Acid Gel Stain (Invitrogen) in 1xTBE for ≥ 30 min in the dark before imaging on the Typhoon. Band intensities were quantified using ImageQuant (Cytiva) and the percentage of RNA bound calculated using Equation 1:

$$RNA_{bound}(\%) = 100 \times \frac{{E_T}^{n_h}}{{K_{D,app}}^{n_h} + {E_T}^{n_h}}$$

Binding data were fit using equations derived from the binding models shown in Figure S10. In general, simpler models were tried first, and if systematic errors remained in the fit, more complex models were used to fit the data. The simplest model used was a Hill curve, Equation 2:

$$RNA_{bound}(\%) = 100 \times \frac{{E_T}^{n_h}}{{K_{D,app}}^{n_h} + {E_T}^{n_h}}$$

In this model, $K_{D,app}$ is the apparent K_D for binding of Pus7 to one of the many sites on a given RNA; $K_{D,app}{}^{n}{}_{h}$ is the concentration of Pus7 at which 50% of available sites are bound. When systematic errors remained in the fit, a more complex model was used in which Pus7 bound first

to a single specific site on the RNA, followed by the binding of multiple Pus7 moieties to multiple nonspecific sites on the same RNA (Figure S10B). These data were analyzed using Equation 3:

$$RNA_{bound}(\%) = 100 \times \frac{\left(E_T / K_{D,app1}\right) \times \left(1 + \left(E_T / K_{D,app2}\right)^{n_h}\right)}{1 + \left(E_T / K_{D,app1}\right) \times \left(1 + \left(E_T / K_{D,app2}\right)^{n_h}\right)}$$

Neither of these models are theoretically correct, in particular because there is no evidence for cooperative binding of Pus7 to RNA. A theoretically correct binding model would need to account for random binding of Pus7 to all of the possible binding sites on a given RNA. Each RNA has many binding sites, which are not all equivalent because of differences in sequence and structure, and the binding sites can interact with one another negatively (via steric occlusion, for example) and positively (e.g. binding of Pus7 at one site changes structure at a second site, increasing binding affinity). Our experimental methods do not provide enough information to develop such a model. The simplified models we use to analyze the data are therefore the best available tool, and allow for quantitative comparison of differences in binding that are identifiable via visual inspection of EMSA gel images.

Single-turnover pseudouridinylation assays

RNA substrates containing 5,6-[^{3}H]-uridine were prepared by *in vitro* transcription (7) and denaturing gel purification. Reaction buffer was as described for the EMSA experiments. RNA substrates were folded in 1X reaction buffer by heating to 60°C for 5 minutes, followed by a 30 minute incubation at 30°C (8). Indicated concentrations of protein were mixed with the smallest detectable amount of substrate (~3,000 cpm per uridine in each timepoint, which allows reliable detection of tritium release above 5% turnover). At each timepoint an aliquot of reaction mix (containing ~3,000 cpm/U) was quenched in 1,250 µL 0.1 M HCl (final) containing 250 µg Norit-A. Quenched timepoints were mixed, centrifuged at 21,000 x *g* for 5 minutes, and 1000 µL of supernatant was transferred to a new tube containing 250 µL of 0.1 M HCl with 250 µg Norit-A. Mixing and centrifugation were repeated, and 1000 µL of the supernatant was filtered through glass wool in a 1 mL pipet tip to remove residual charcoal. Aliquots of the filtrate (500 µL) were removed for liquid scintillation counting in a Beckman LSC-6500. For each reaction mix, input controls were prepared by passing an aliquot of reaction through the same process using 0.1 M HCl without the Norit-A. Counts observed in the input sample are used to calculate cpm/uridine, allowing calculation of the amount of Ψ produced at each timepoint. Background counts were determined by processing an RNA only reaction aliquot through the sample pipeline; these counts were routinely equivalent to background in our instrument (~30 cpm). Fraction of target U converted to Ψ data were fitted using Equation 4:

$$U > \Psi\ (fraction) = 1 - e^{-k_{obs} \times t}$$

Stop Flow Assays: Pus7/ D256A binding with fluorescently labeled mRNA

D256A Pus7 and 5'-fluorescein labeled CDC8 were generated and purified as described as above. Kinetic binding experiments were performed using the Kintek SF-300x stop-flow apparatus. Fluorescently labeled mRNA (5 nM final concentration) was mixed with D256A at

varied concentrations (20 nM – 750 nM final). Binding experiments were performed at room temperature in same buffer used in the EMSA experiments over the span of 1-1.5 seconds. Lower concentrations of Pus7/D256A (0-100nM) displayed monophasic behavior and were fit with a single exponential equation: $A_1e^{-k1t} + c$ to obtain a k_{obs1}. Higher concentrations displayed biphasic behavior and therefore were fit with a double exponential equation: $A_1e^{-k1t} + A_2e^{-k2t} + c$ to obtain k_{obs1} and k_{obs2}. The k_{obs1} values from both fits were then plotted against the concertation of D256A PUS7 mutant, displaying a linear relationship. The y-intercept gave a k_{off} of approximately 35 s^{-1} and the slope gave a k_{on} of ~4.3 x 10^8 $M^{-1}s^{-1}$. The K_D For D256A binding CDC8 was obtained using Equation 5: $K_D = k_{off}/k_{on}$.

Wild-type and *pus7*Δ growth assessment

Wild-type and *pus7*Δ yeast cells were inoculated into 3 mL YPD media and grown overnight. Then, they were diluted to OD_{600}=1 as a starting point, and 7 ml of 10-fold serial dilutions were spotted on fresh YPD agar plates supplemented with 0.75-1.0 M NaCl, 250 mM $MgSO_4$, 200 mM puromycin, 100 ng/mL cycloheximide, 25-50 mg/mL hygromycin B, 50 mM MG132 and 1.5-3 mg/mL paromomycin. Growth of the cells were also tested in the presence of different carbon sources including 2% glucose, 2% sucrose and 2% galactose in YEP agar media (1% yeast extract and 2% peptone). The plates were incubated for 2-3 days at 30°C unless otherwise indicated.

Phylogenetic tree generation

Annotated TruD/Pus7 sequences (>400 total sequences) from GenBank (NCBI) were aligned using ClustalW. Then, a representative 44 amino acid sequence was used for further analysis. Evolutionary analyses were conducted using MEGAX tool (9). The phylogenetic tree was generated using the Maximum Likelihood method (10). The bootstrap consensus tree inferred from 100 replicates is taken to represent the evolutionary history of the taxa analyzed (11). The percentage of replicate trees in which the associated taxa clustered together in the bootstrap test (100 replicates) are shown next to the branches. Initial tree(s) for the heuristic search were obtained automatically by applying Neighbor-Join and BioNJ algorithms to a matrix of pairwise distances estimated using the JTT model, and then selecting the topology with superior log likelihood value. A discrete Gamma distribution was used to model evolutionary rate differences among sites (5 categories (+G, parameter = 1.3722)). The rate variation model allowed for some sites to be evolutionarily invariable ([+I], 0.89% sites). There were a total of 1344 positions in the final dataset.

Ribosome profiling data analysis

Raw ribosome profiling sequencing data from two studies (12, 13) were downloaded and processed using the procedures described below. Briefly, adapter contaminations and low-quality reads were filtered out from the raw reads using the Cutadapt tool (14) like as previously described (15). Subsequently rRNA and tRNA contaminations were removed by aligning reads to the non-coding RNA (ncRNA) sequences of *S. cerevisiae* using Bowtie2 (16). Next, the remaining unaligned sequences were aligned against the transcriptome (coding RNA) of *S. cerevisiae* (R64-1-1 genome built) using TopHat2 (17). After that perfect match alignments were extracted from the TopHat output. For further downstream analysis, 3'- and 5'-end P-site offset values were

determined using riboWaltz (18). These P-site offset values are required to identify where ribosomes are located on each ribosome protected footprints (RPFs). After P-site offset calculation, actively translating ribosomes that represent trinucleotide periodicity were identified. Then the number of mapped RPFs was counted for each codon position within a gene using Samtools (19).

Modeling of thermal stability of PUS7

Using the established relationship between a protein's stability and its heat capacity (ΔC_p), stability (ΔG) chain length can be reasonably modeled as a function of chain length (N) and temperature (T) (26-29). Pus 7's stability curve was modeled as a function of N and T using previously published model seen in, Equation 6 (27, 29-31).

$$\Delta G(N,T) = \Delta H_R + \Delta C_p(T - T_R) - T\Delta S_R - T\Delta C_p \; ln \; ln \left(\frac{T}{T_R}\right) \quad (6)$$

Where enthalpy (ΔH_R) and entropy (ΔS_R) are calculated at a reference temperature and (ΔC_p) is the heat capacity of a protein, T_R is the reference temperature of 373 K for both ΔH_R and ΔS_R. These previous studies took advantage of the correlation between a protein's thermodynamic parameter and chain length to derive linear equations from experimental measurements collected into databases. The linear equations can be expressed as equations 7, 8, 9, (27, 29)

$$\Delta H_R = m_h \cdot N + b_h \quad (7)$$

$$\Delta S_R = m_s \cdot N + b_s \quad (8)$$

$$\Delta C_p = m_c \cdot N + b_c \quad (9)$$

Where m_h and b_h are the slope and intercept of ΔH_R, m_s and b_s are the slope and intercept of ΔS_R and m_c and b_c are the slope and intercept of ΔC_p when these parameters are plotted as a function of *N*. Equations 7, 8, 9 can be inserted into Equation 6, in order to get stability as a function of N and T as seen in Equation 10.

$$\Delta G(N, T) = \quad (10)$$
$$(m_h N + b_h) + (m_c N + b_c)(T - T_R) - T(m_s N + b_s) - T(m_c N + b_c) \; ln\left(\frac{T}{T_R}\right)$$

Detection and quantification of pseudouridylation: CLAP assay

The CLAP assay was adapted from Zhang, 2019 (25).

Pseudouridylation of total RNA or *in vitro* transcribed CDC8

Briefly, 150 μg of total RNA purified from BY4741 yeast *Δpus7::kanMX* was mixed with 50 μM Pus7-WT or Pus7-ΔID1 and incubated for 10 minutes at 30°C or 37°C in 1X pseudouridinylation buffer (100 mM TRIS-HCl pH 8.0, 100 mM NH_4OAc, 2 mM DTT, 5 mM $MgCl_2$) to modify the RNA. The reaction was stopped by adding 1/10th volume of 3 M NaOAc pH 5.2, followed by two phenol:chloroform (1:1) extractions with saturated acid phenol, and a final chloroform extraction to isolate the RNA. The RNA was then precipitated by adding an equal volume of 100% EtOH and 1 μL of GlycoBlue (Thermo Fisher, AM9515) and incubated at -20°C for 3 hours.

CMC treatment

RNA was resuspended in 41.5 μL of BEU buffer (50 mM Bicine pH 8.3, 4 mM EDTA, 7 M Urea). For CMC treated samples, 8.5 μL of freshly prepared 1 M CMC dissolved in BEU buffer was added, for a final concentration of 170 mM CMC. For CMC non-treated samples, 8.5 μL of BEU buffer was added, for a final reaction volume of 50 μL. Samples were incubated at 37°C for 20 minutes. The reaction was stopped by adding 100 μL of Stop Buffer (300 mM NaOAc pH 5.2, 0.1 mM EDTA) for a final volume of 150 μL. Excess CMC was removed by two sequential ethanol precipitations. Briefly, 700 μL 100% EtOH, and 1 μL GlycoBlue were added to the reaction before incubating 3 hours at -20°C. Sample was spun down for 30 min, 15kRPM, at 4°C before removing the supernatant, and washing the pellet by adding 500 uL of 70% EtOH, and spin for 5 min at 15kRPM. Remove supernatant and allow pellet to dry. Resuspend the RNA pellet in 100 μL of Stop Buffer and repeat ethanol precipitation and wash.

Alkali Treatment

Resuspend the pellet in 40 μL of 50 mM Na_2CO_3 pH 10.4 (pH taken at 37°C, temperature of incubation) and incubate for 3 hours at 37°C. Precipitate RNA via ethanol precipitation, as described above, with an additional 70% ethanol wash. Let pellet air dry. Resuspend the pellet in 20 μL sterile water and determine concentration by nano-drop.

RNA 5' Phosphorylation

To 6 μg RNA in 6.5 μL, add 1 μL 10X T4 PNK reaction buffer (NEB B0201S), 1 μL of 1 mM ATP, 0.5 μL 20 U/μL SUPERase•In RNase Inhibitor (Thermo Fisher AM2694), and 1 μL 10 U/μL T4 PNK (NEB M0201L) for a final volume of 10 μL. Incubate at 37°C for 30 minutes.

Blocker Ligation

To the reaction above, add 1 μL 10X T4 RNA Ligase reaction buffer (NEB B0216L), 1 μL of 100 μM 5' RNA blocker oligo (IDT /5AmMC6/rArCrCrCrA), 1 μL of 1 mM ATP, 1 μL 20 U/μL SUPERase•In RNase Inhibitor (Thermo Fisher AM2694), 3 μL DMSO, 2 μL sterile water and 1 μL 10 U/μL T4 RNA Ligase I (NEB M0204L) for a final volume of 20 μL. Incubate at 16°C for 16 h. Stop ligation reaction by adding 1.2 μL 200 mM EDTA.

Reverse transcription

For reverse transcription, the RT primer was first annealed by taking 3 μL of ligation mixture, adding 1 μL of 10 X annealing buffer (250 mM Tris-HCl, 480 mM KCl, pH 7.4) and 1 μL of 0.5 μM target specific reverse transcription primer (IDT). Samples were heated to 95°C for 3 minutes and slowly cooled to 37°C at a rate of -0.01°C/s (~15 min). To annealed sample, add 5 μL of 2 X AMV reverse transcription reaction mixture (1.2 U/μL AMV RT (NEB M0277L), 2X AMV RT buffer, and 1 mM of each dNTP) for a final concentration of 0.6 U/μL AMV RT, 1X AMV RT buffer, and 0.5 mM of each dNTP. Incubate at 42°C for one hour. Inactivate AMV RT by heating to 85 °C for 5 min before placing on ice. To digest RNA, add 1 μL of 5 U/μL RNaseH and incubate at 37°C for 20 minutes. Inactivate RNaseH by heating to 85 °C for 5 min and before placing reaction on ice. Add 1 μL of splint/adaptor oligo mix (1.5 μM adaptor oligo, 1.5 μM splint oligo) and incubate mixture at 75°C for 3 minutes followed 3 minutes at room temperature to anneal the splint/adaptor.

Add 4 μL of 4x ligation mixture (40 U/μL T4 DNA ligase, 4X T4 DNA ligase buffer, and 50% DMSO) for a final concentration of (10 U/μL T4 DNA ligase, 1X T4 DNA ligase buffer, and 12.5% DMSO). Incubate at 16°C for 16 h. Heat reaction to 65°C for 10 min to deactivate T4 DNA ligase, place immediately on ice.

PCR

Use 2 μL of reaction above, mix with 3.5 μL of 5 μM forward primer and 3.5 μL of 5 μM reverse primer (or reverse transcription primer). Add components for Q5 DNA polymerase reaction to a final volume of 35 μL and final concentration of 1X Q5 reaction buffer, 1X Q5 GC enhancer, 200 μM of each dNTP, 0.5 μM of forward and reverse primers, and 0.2 U/μL Q5 high fidelity DNA polymerase (NEB M0491L). Perform 35 cycles of PCR at requisite annealing temperatures for each site. 5 μL of PCR reaction was mixed with 1 μL of 6X TriTrack DNA loading dye and loaded on to a native 10% acrylamide (29:1) gel in 1X TBE pre-run at 10V/cm for 1 hour. Gel ran 3 hours at 10V/cm before being stained in 1X SYBR gold nucleic acid gel stain in 1X TBE for ~10 minutes. Gels were imaged on Amersham Typhoon imager and quantified using ImageQuant.

CLAP Primers

ARG5,6_RT	CCCATAGCAAGATTAATATTT
ARG5,6_FWD	TAGTTATTGGTGGTTTCA
ARG5,6_REV	TGCAGACATTGAGTAGC
ARG5,6_ADAPT	pCCATGTGAAACCACCAATAACTA
ARG5,6_SPLINT	TTTCACATGGAGTTGTTTGC/3SpC3/
BET2_RT	GCTTGAGCTGCATGGGATTCA
BET2_FWD	ACTATCAATTTTGGGTGAATTAA
BET2_REV	GCATTAGGACATAATCCAAAG
BET2_ADAPT	pCCATGTTAATTCACCCAAAATTGATAGT
BET2_SPLINT	ATTAACATGGAGACTTTGTA/3SpC3/
U2snRNA_RT	TATTATTTTGGGTGCCAAAAA
U2snRNA_56_FWD	CCTTTTGGCTTAGATCAA
U2snRNA_REV	ATGTGTATTGTAACAAATTAAAAGG
U2snRNA_56_ADAPT	pCCATGTTGATCTAAGCCAAAAGG
U2snRNA_56_SPLINT	ATCAACATGGAACAACTGAA/3SpC3/
U2snRNA_35_FWD	ACGAATCTCTTTGCCTTT
U2snRNA_35_ADAPT	pCCATGAAAGGCAAAGAGATTCGT
U2snRNA_35_SPLINT	CCTTTCATGGAGTATCTGTT/3SpC3/
CDC8_RT	ATATGCGTACTCAAAACAGGC
CDC8_FWD	GCTATTGGATAAAGAGATAAGGA
CDC8_REV	TCAACGATTTGCCAAATAAGC
CDC8_ADAPT	pCCATGTCCTTATCTCTTTATCCAATAGC
CDC8_SPLINT	AAGGACATGGAGACGTTACT/3SpC3/

EFB1/TEF5_81_RT	GTTGAACCATCTGGAGAATTC
EFB1/TEF5_81_FWD	GAAACAATTAAACGCTTCTTT
EFB1/TEF5_81_REV	TGGGTAAGCAGATTGGAAA
EFB1/TEF5_81_ADAPT	pCCATGAAAGAAGCGTTTAATTGTTTC
EFB1/TEF5_81_SPLINT	TCTTTCATGGACTGCTGTTT/3SpC3/
RTC3_77_RT	TCCTGAGGAGTGAAAACTTCG
RTC3_77_FWD	GGTGAAAATACAGATTTGATTG
RTC3_77_REV	AAGAGTTCGACAACTTCAGAT
RTC3_77_ADAPT	pCCATGCAATCAAATCTGTATTTTCACC
RTC3_77_SPLINT	GATTGCATGGAGACGAATAT/3SpC3/
RTC3_288_RT/REV	TCAATTGTAGGCTTTGGTTC
RTC3_288_FWD	GTTATCGATTTGATATTGAGAAA
RTC3_288_ADAPT	pCCATGTTTCTCAATATCAAATCGATAAC
RTC3_288_SPLINT	AGAAACCATGGAGTCTCAAAA/3SpC3/
TEF2_555_RT	GGACTTCAAGAACTTTGGATG
TEF2_555_FWD	GAAACCTCCAACTTTATCAA
TEF2_555_REV	GGTGGTAGCTTCAATCATGTT
TEF2_555_ADAPT	pCCATGTTGATAAAGTTGGAGGTTTC
TEF2_555_SPLINT	ATCAACATGGGTTCCATTCG/3SpC3/
TEF2_1104_RT	ACCCTTGTACCATGGAGCGTT
TEF2_1104_FWD	TTACTCTCCAGTTTTGGA
TEF2_1104_REV	GTCTTCCAACTTCTTACCAGA
TEF2_1104_ADAPT	pCCATGTCCAAAACTGGAGAGTAA
TEF2_1104_SPLINT	TTGGACATGGAGATTCGACG/3SpC3/

SUPPLEMENTAL APPENDIX FIGURES

Figure S1: Phylogenetic relations in TruD and Pus7 family. This tree shows the relation of Pus7 family proteins in different species. It also represents the relation between Pus7 family with TruD family proteins.

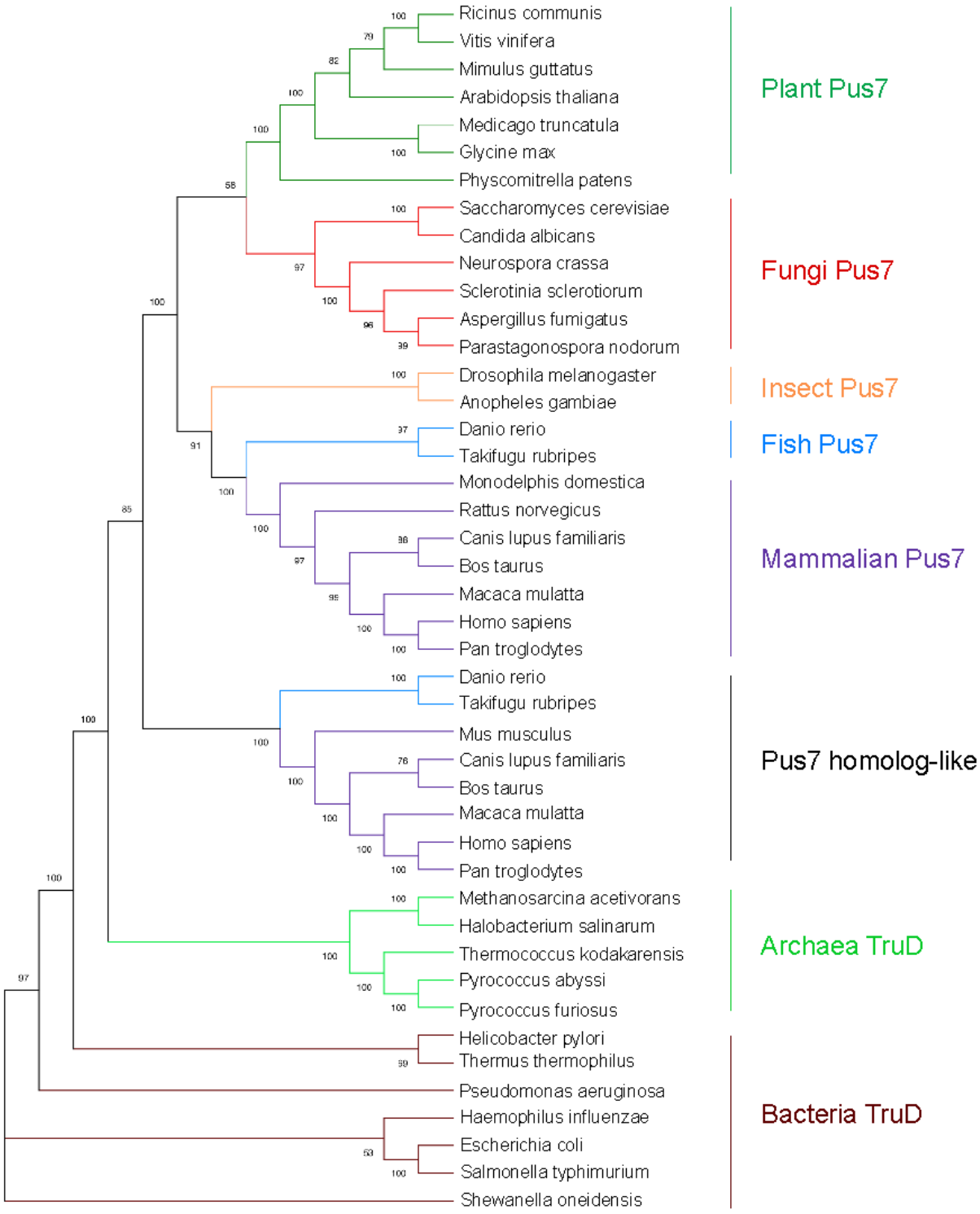

Figure S2: Comparison of Pus7 structures. (A) Rendering of the electrostatic surface potential of yeast Pus7 generated with ABPS Electrostatics (20). Negatively charged regions are shown in red, and positively charged regions are shown in blue. **(B)** Catalytic residue D256, Pus7 numbering, is shifted ~4A relative to the same residue in TruD (D80). Figure shows alignment of the yeast Pus7 active site (purple) and residues (gray) with the equivalent residues in TruD (yellow, PDB: 1SB7)(21). Pus7 numbering in black, TruD numbering in yellow. Distances measured both from CAlpha position and from the carboxyl on D256/D80. **(C)** Superposition of yeast Pus7 (light gray, blue) and human Pus7 (dark gray, yellow, PDB: 5KKP)(22), (C_{alpha} RMSD = 3.743 for 144 atoms) and rotated 180 degrees to show the difference in position of the insertions (I, II, and III) in yeast (blue) and human (yellow) Pus7. The catalytic residue D256, yeast numbering, is shown in the active site (light gray spheres). **(D)** Top down view of yeast and human superposition, looking down into the active site. **(E)** Putty representation of Pus7 colored according to B factors. Residues with the lowest B factors in blue (min = 20Å) and maximum in red (max=200Å). (**F)** 2Fo-Fc maps showing experimental electron density (gray mesh) around yeast Pus7 ID-I (blue) contoured at 1.5σ. Methionine residues (M88 and M145, orange), shown as sticks, used for SAD phasing.(**G**) Superposition (using 136 – 336 c-alpha atoms of the TRUD and PUS domains, RMSD: ~2.52Å for these domains) of TruD homologs, including: each molecule in the asymmetric unit of each *E.coli* TruD structure (gray, PDB: 1sb7, 1si7, 1szw), both TruD molecules in the asymmetric unit of the *Methanosarcina Mazei* structure (gray, PDB: 1z2z), the single Pus7 molecule in the human structure (yellow, PDB: 5kkp), and the single molecule in the yeast Pus7 structure reported here (blue).

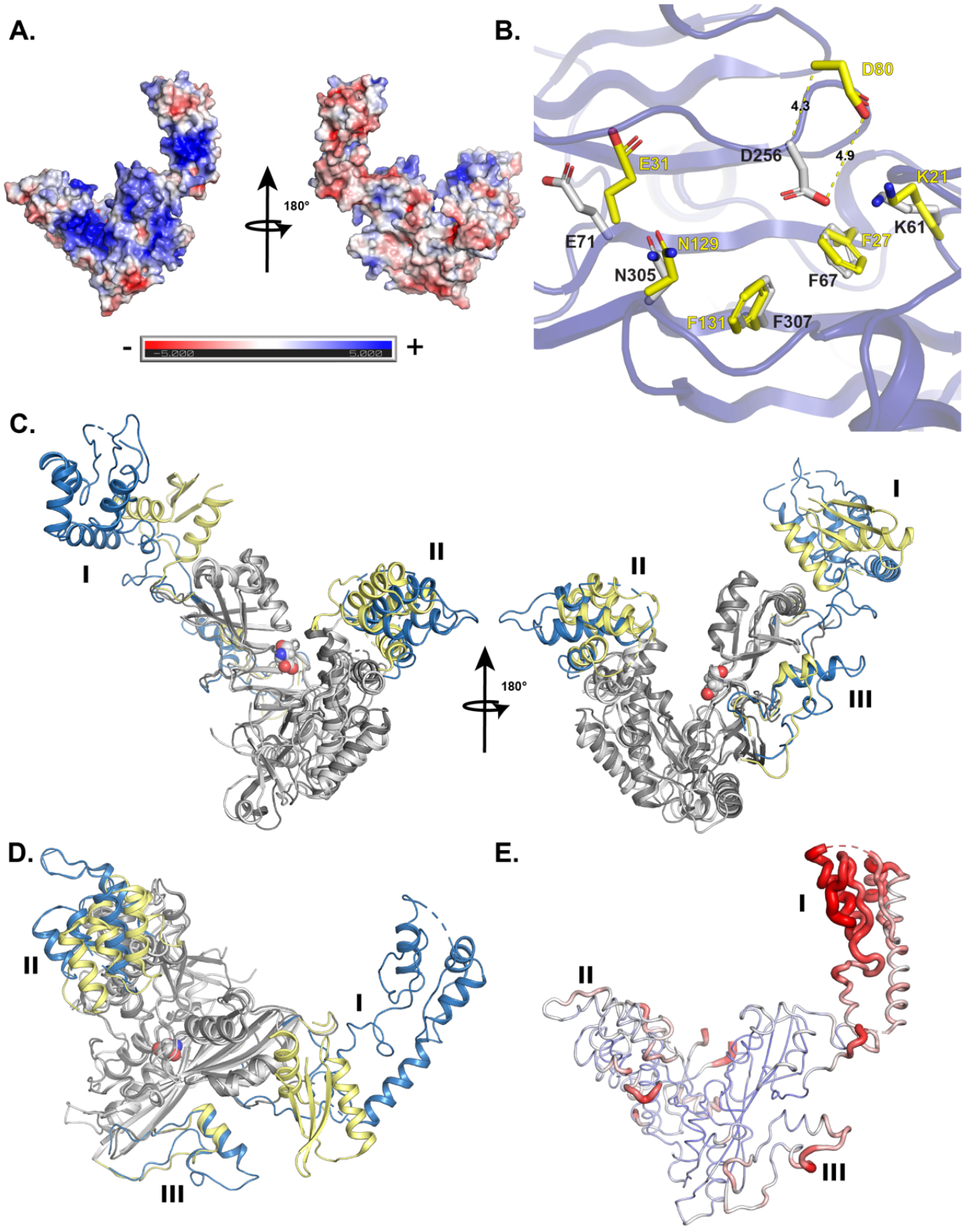
A.
180°
-
-5.000
5.000
+
B.
D80
4.3
E31
D256
4.9
K21
K61
E71
N129
F27
N305
F67
F131
F307
C.
I
II
180°
I
II
III
D.
II
I
III
E.
I
II
III

F

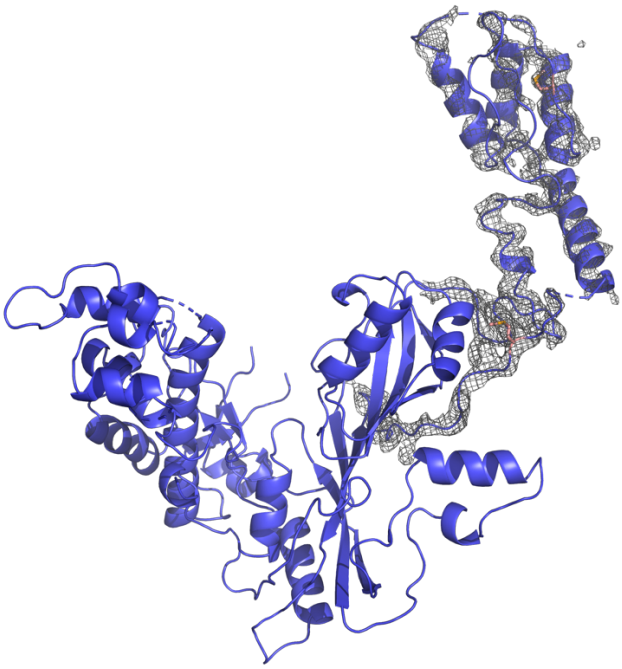

G

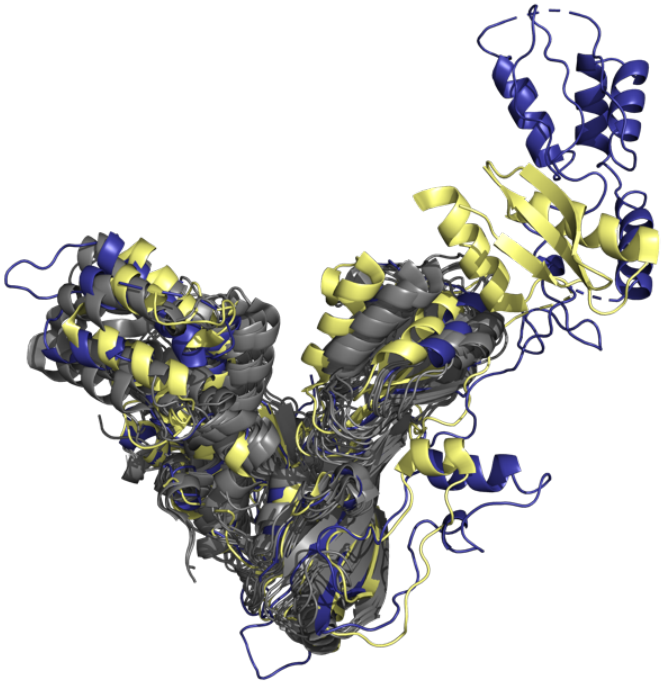

Figure S3: Sequence alignment of representative TruD family members.

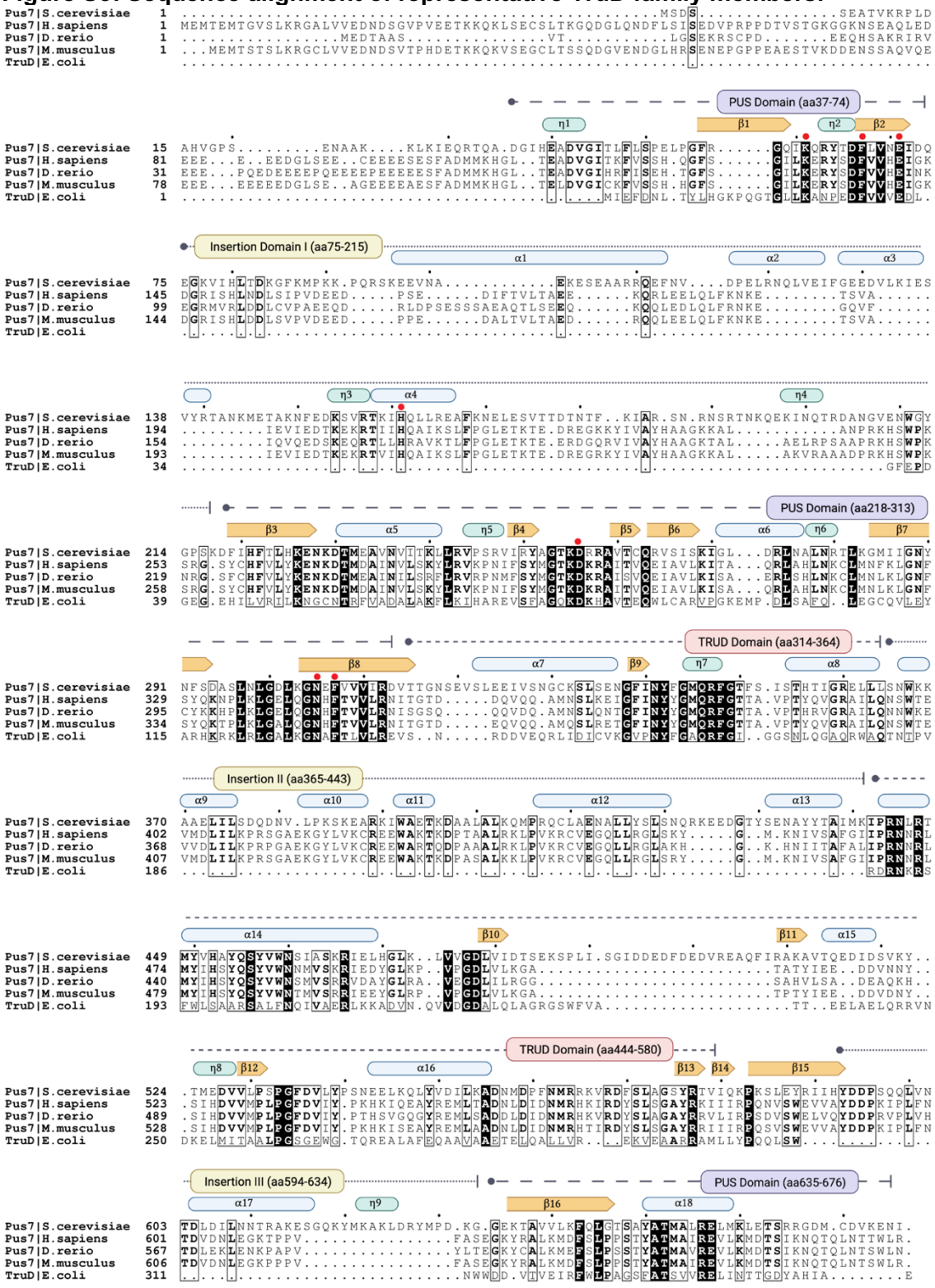

Figure S4: ID-I contains a single strand nucleic acid binding R3H domain. DALI alignment of the R3H motifs (based on 56 atoms, RMSD: 2.788 Å) from humanPus7 ID-I (yellow, PDB: 5kkp) and PARN (blue, PDB: 2a1s).

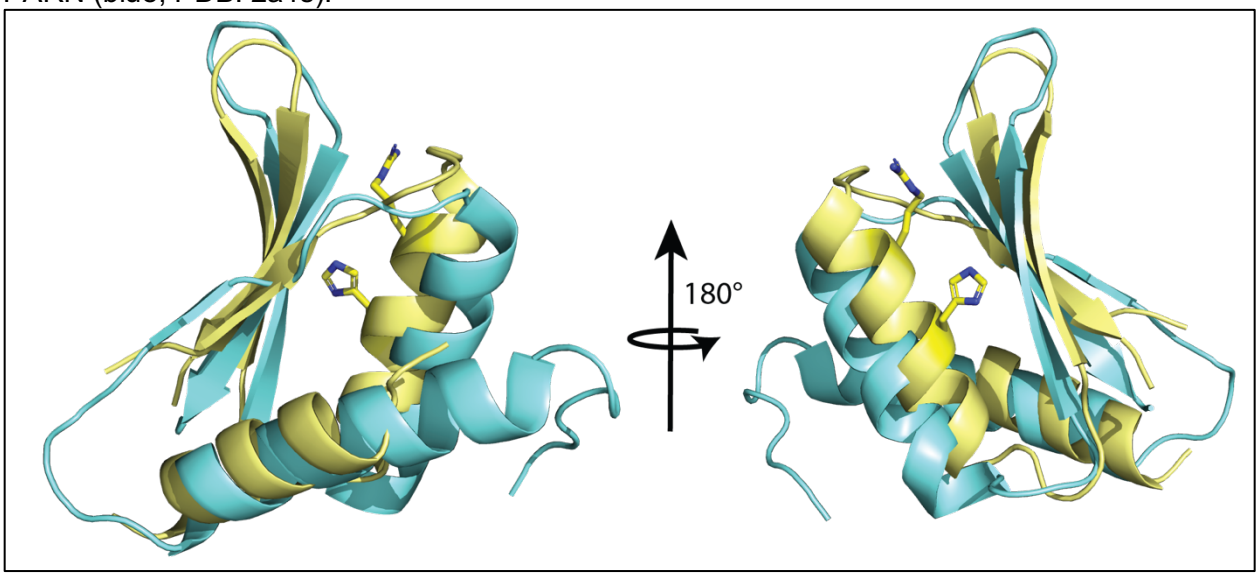

Figure S5: *S. cerevisiae* cell growth under different conditions.

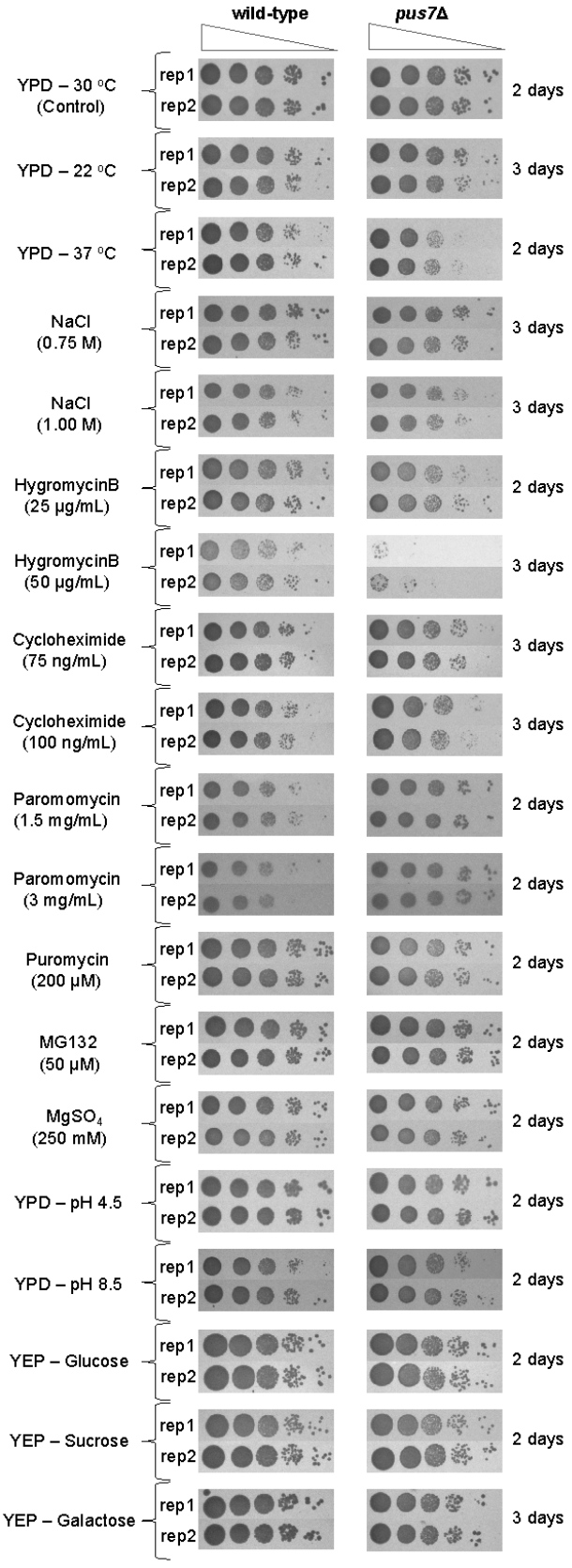

Figure S6: Example S. cerevisiae cell growth in liquid media. Growth curves for wild-type and *pus7*Δ cells in YPD at 30°C after the addition of **(A)** nothing, **(B)** cycloheximide, and **(C)** paromomycin.

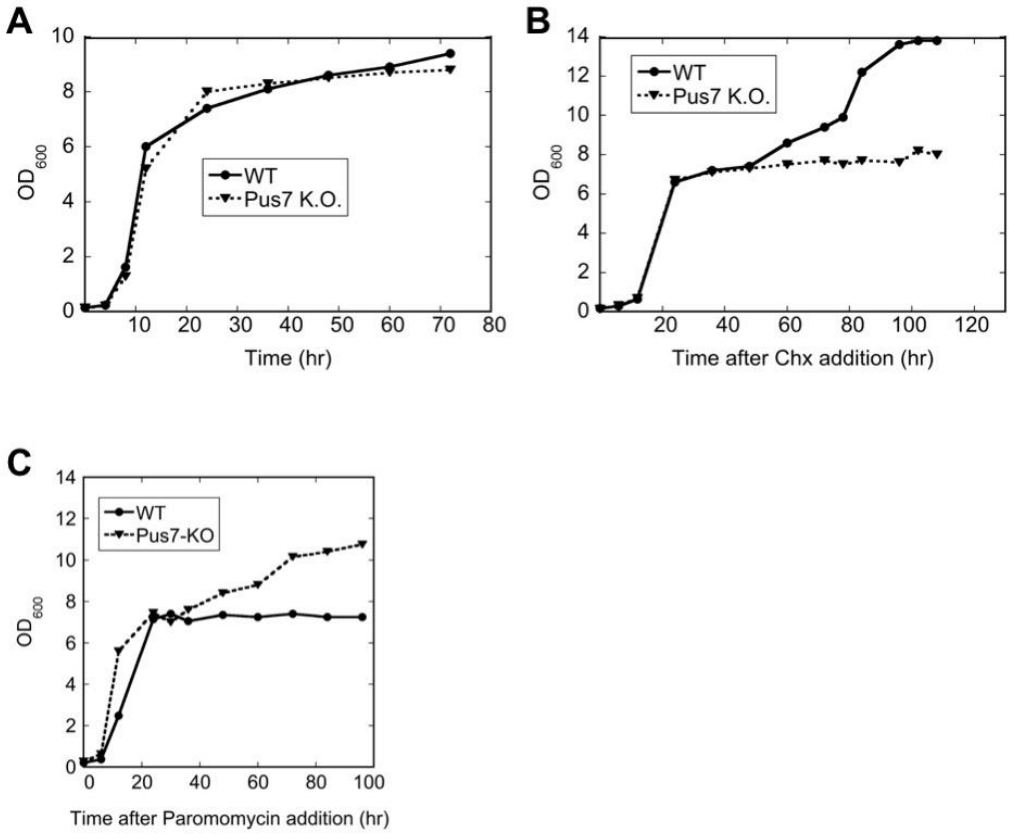

Figure S7: Ribosome occupancies are affected in the absence of Pus7. (A) Ribosome protected footprint (RPF) read length distribution. Distribution of ribosome protected fragments (RPFs) length show that most of the RPFs are between 27-30 nucleotide length. **(B)** ~50-60 % of these RPFs are in-frame (frame 0) **(C)** Ribosome occupancies are altered in p*us7*Δ compared to wild-type cells. Fold change in the ribosome codon occupancies was simply calculated by dividing the number of mapped RPFs in the P-site of *pus7*Δ to wild-type.

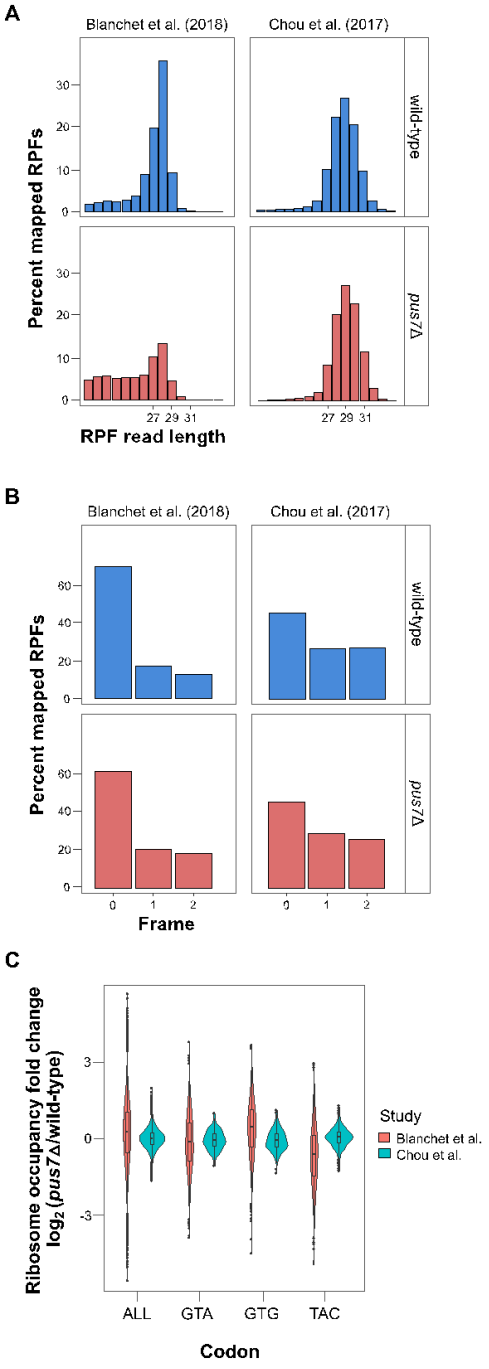

Figure S8: Raw EMSA data

Each panel is titled “SUBSTRATE PROTEIN” in bold text. Panels are grouped by substrate and then by protein mutations. Each panel shows the binding model used for curve fitting, one gel image, and a single curve fitted to all replicate data sets. The dissociation constant for the specific binding step of the model is noted along with the error of the fitted parameter.

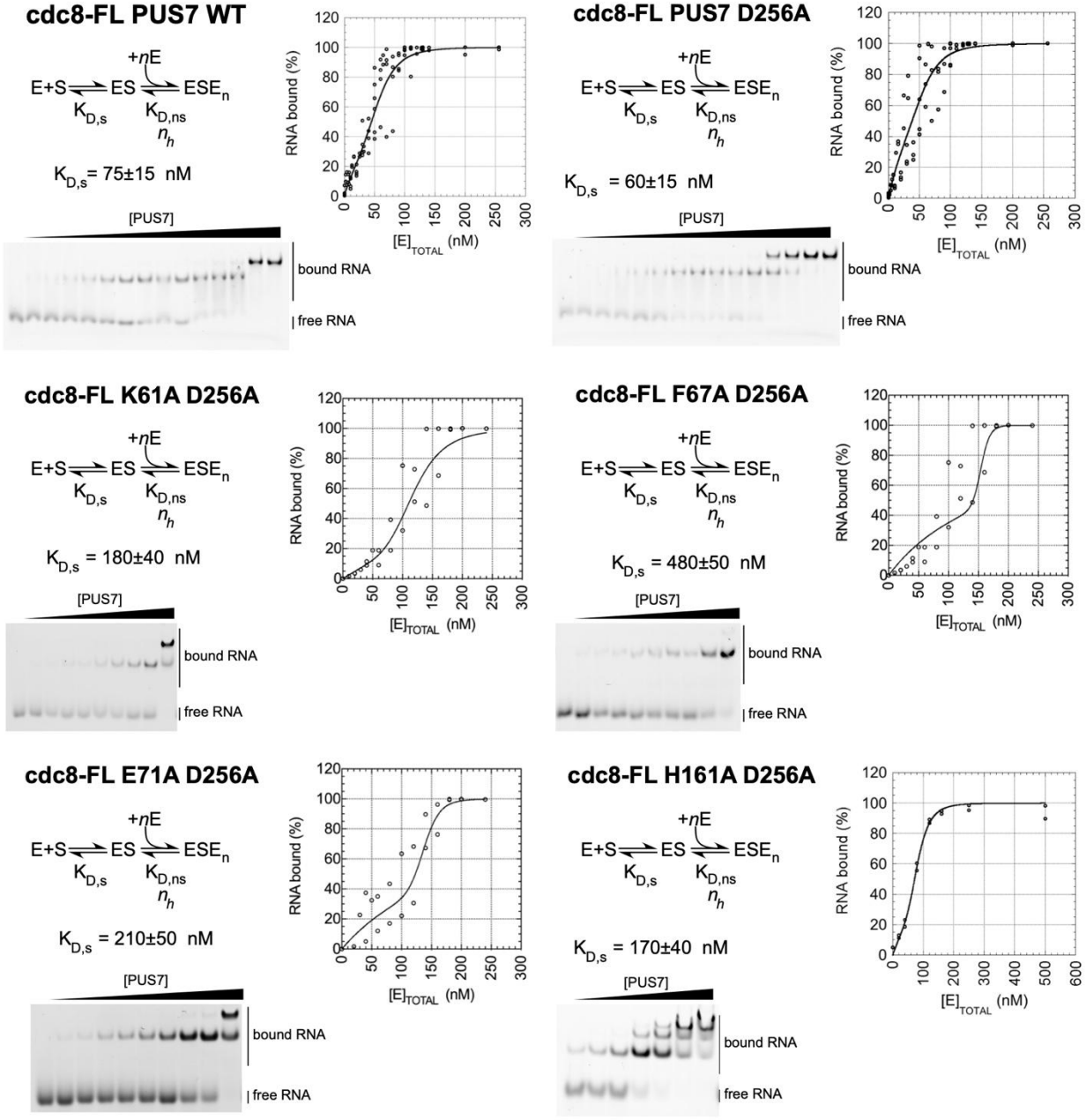

cdc8-FL N305A D256A

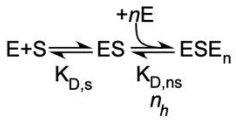

$K_{D,s}$ = 230±60 nM

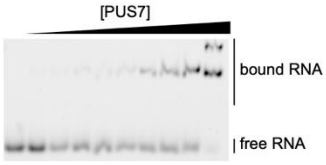

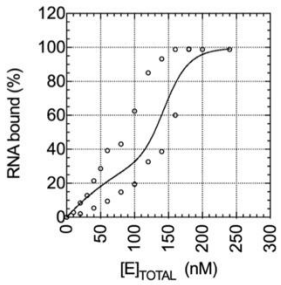

cdc8-FL F307A D256A

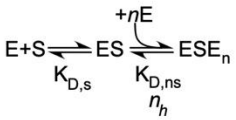

$K_{D,s}$ = 340±170 nM

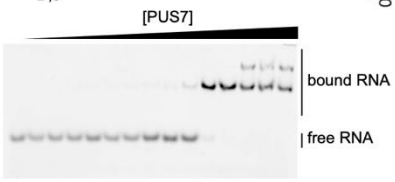

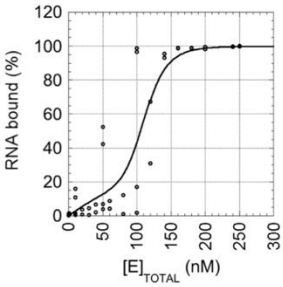

cdc8-FL ΔID1 D256A

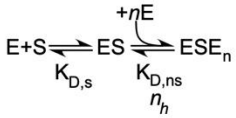

$K_{D,s}$ = 160±40 nM

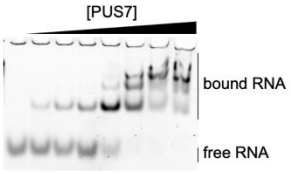

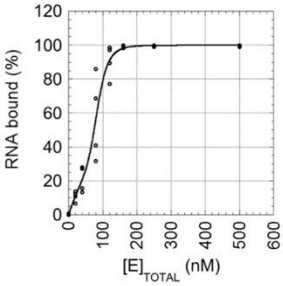

cdc8-FL nontarget D256A

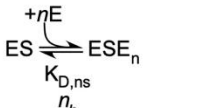

nontarget: UG**C**AG
target: UG**U**AG

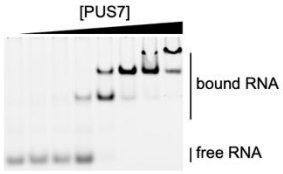

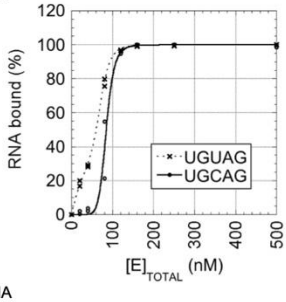

cdc8-A PUS7 WT

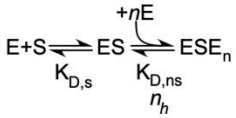

$K_{D,s}$ = 15±2 nM

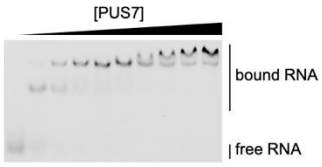

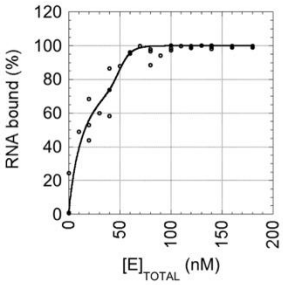

cdc8-A PUS7 D256A

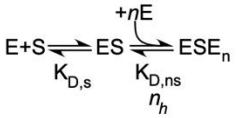

$K_{D,s}$ = 57±4 nM

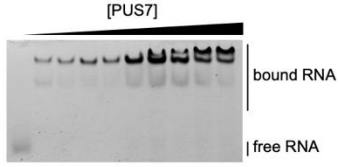

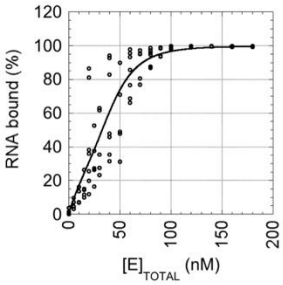

cdc8-B PUS7 WT

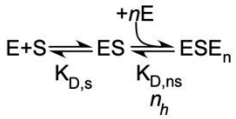

$K_{D,s}$ = 630±1500 nM

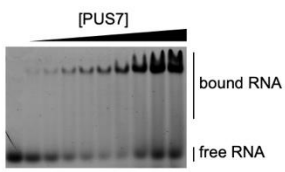

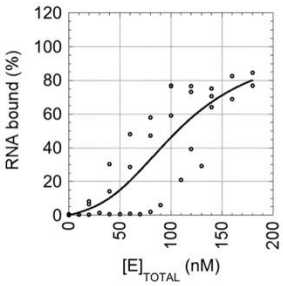

cdc8-B PUS7 D256A

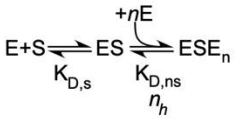

$K_{D,s}$ = 800±320 nM

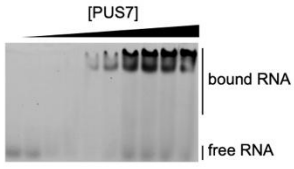

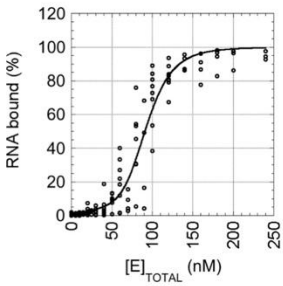

cdc8-C PUS7 WT

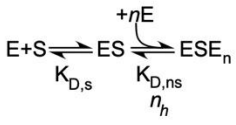

$K_{D,s}$ = 74±18 nM

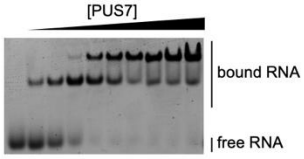

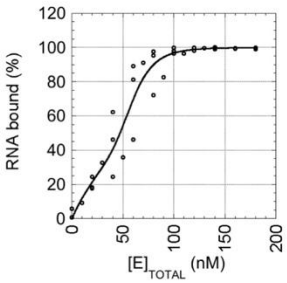

cdc8-C PUS7 D256A

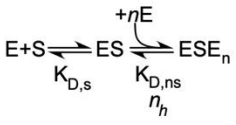

$K_{D,s}$ = 130±13 nM

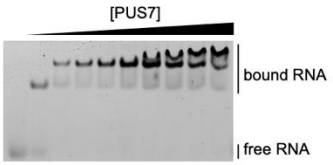

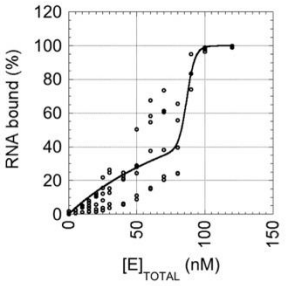

tArg PUS7-WT

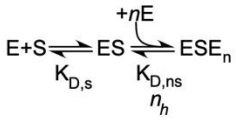

$K_{D,s}$= 550±160 nM

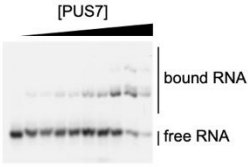

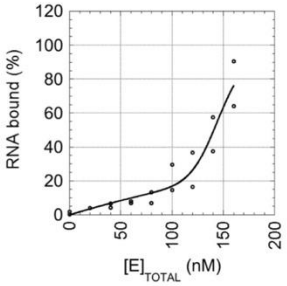

tArg PUS7-D256A

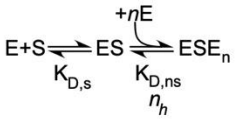

$K_{D,s}$= 700±170 nM

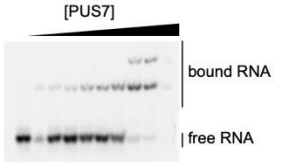

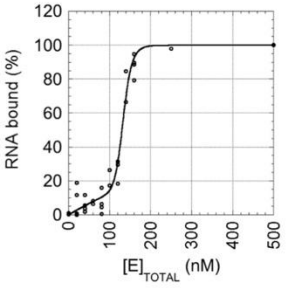

tArg-C13U PUS7-WT

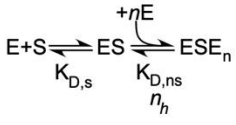

$K_{D,s}$= 470±180 nM

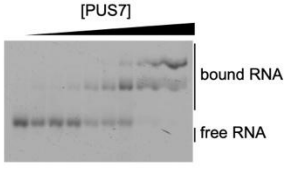

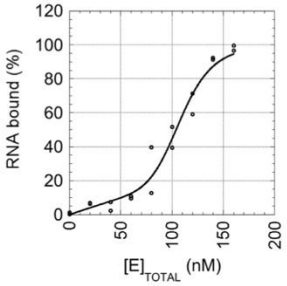

tArg-C13U PUS7-D256A

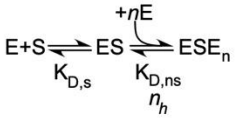

$K_{D,s}$ = 120±20 nM

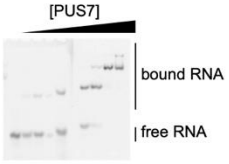

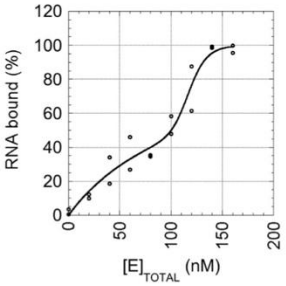

tAsp PUS7-D256A

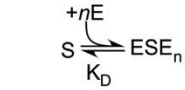

K_D = 16±1 nM

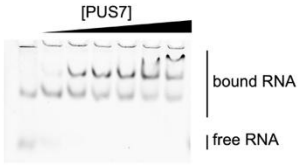

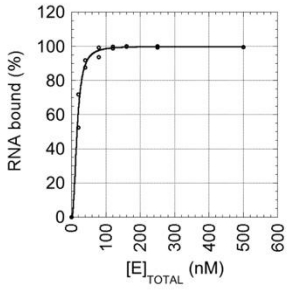

tAsp PUS7-ΔID1 D256A

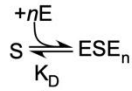

K_D = 34±1 nM

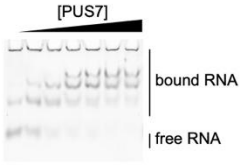

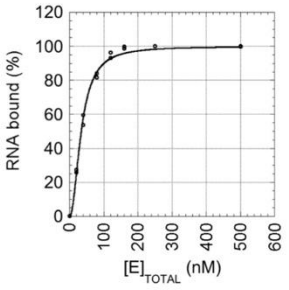

ST1 PUS7-D256A

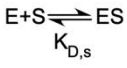

$K_{D,s}$ = 34±4 nM

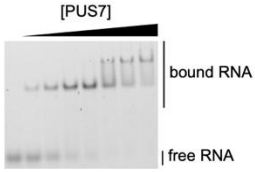

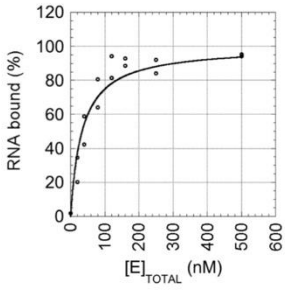

ST1 PUS7-ΔID1 D256A

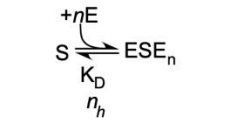

K_D = 54±3 nM

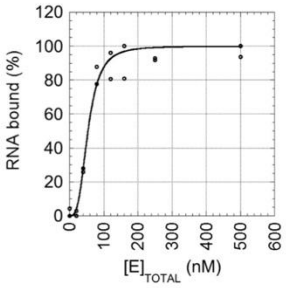

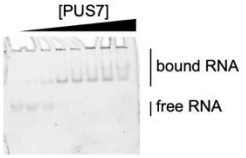

SNT1 PUS7 D256A

K_D = 47±2 nM

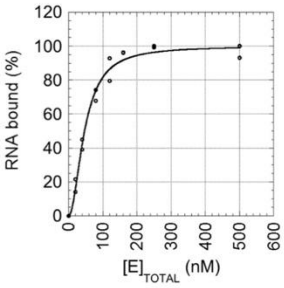

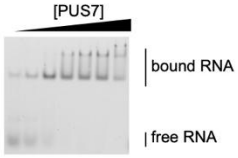

ST2 D256A

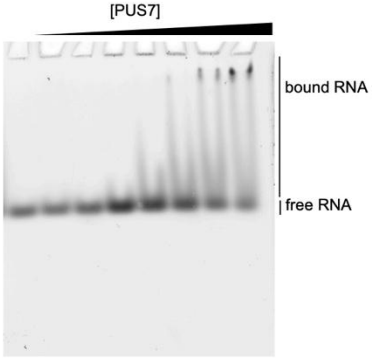

binding not quantitatively analyzed

ST2 PUS7-ΔID1 D256A

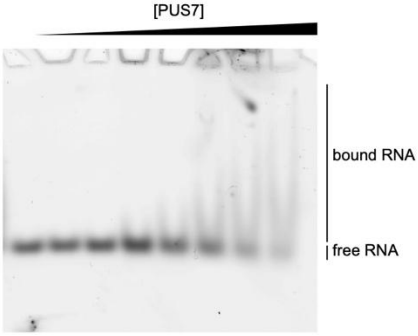

binding not quantitatively analyzed; however there is less bound (smeared) RNA with ΔID1 relative to D256A alone

Figure S9: Yeast PUS1 nonspecifically binds RNA and catalyzes pseudouridinylation outside its consensus sequence. A. EMSA using PUS1 and its GLK1 target RNA showing specific and nonspecific binding events. B. Measurement of pseudouridine synthase activity on a variety of PUS7 and PUS1 substrate RNAs. The tRNA substrates are positive controls and show the expected pattern of activity. The MFKKX substrate contains two UGUAG motifs and mutation of one of them eliminates pseudouridinylation at that site by both PUS1 and PUS7.

A

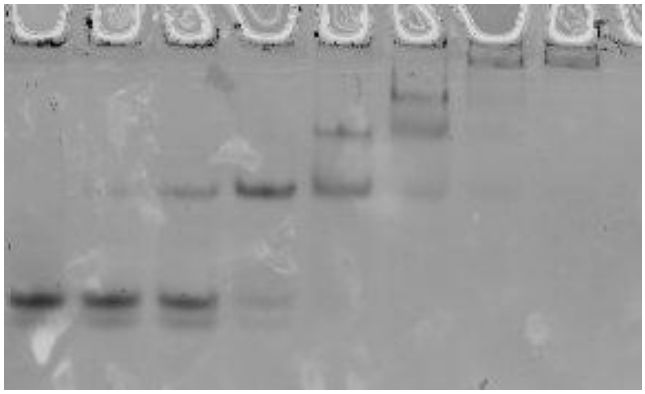

B

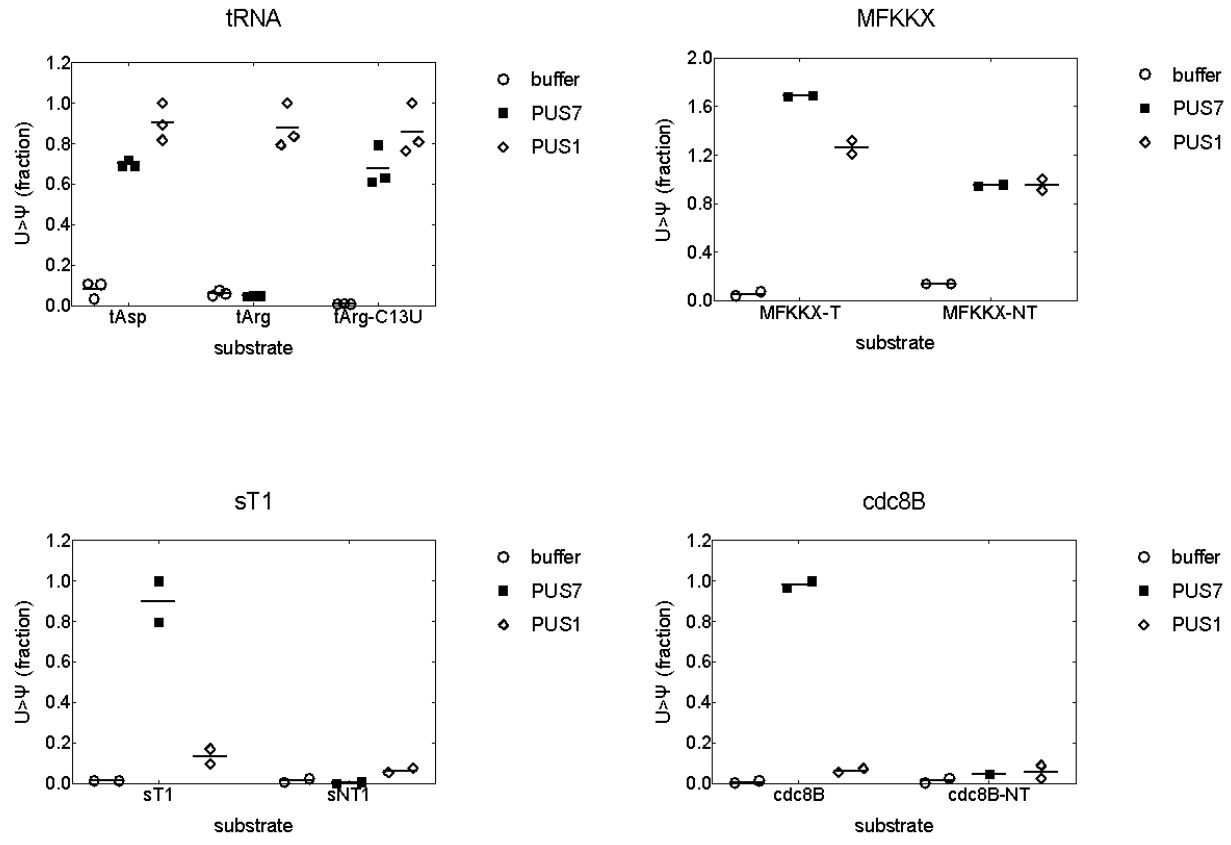

Figure S10: Models utilized in analysis of EMSA data. (A) Simultaneous binding of *n* PUS7 enzymes to a single RNA substrate, otherwise known as a Hill binding curve. This model was used when no specific binding was apparent. Binding curves were fit to the equation shown. The EMSA assay allowed direct estimation of free enzyme concentrations, so we fit the data using both free and total enzyme concentrations. The differences between these fits was much smaller than the difference in fits of data from independent replicates. Since using total enzyme as the independent variable was not the limiting factor in the precision of our measurements, we used total enzyme as the independent variable for simplicity. (B) Model for binding of one PUS7 enzyme to a single specific site on the substrate RNA, followed by simultaneous binding of *n* PUS7 enzymes to *n* non-specific sites on the same RNA. This model was used to fit data when the Hill equation underestimated the fraction bound at lower concentrations of enzyme, reflecting the existence of a unique site with a lower K_D for PUS7. (C) A realistic model for binding of one or more PUS7 enzymes, in arbitrary order, to a single specific site and one or more nonspecific sites on a single RNA. Occupancy of nonspecific sites is indicated by superscripts *i*, *j*, *k*, … on the S. Nonspecific sites can be bound in any order (e.g., *k,l,l,j*) but are depicted in alphabetical order for convenience.

A

$$S_f + n\,E_f \overset{K_{D,app}}{\rightleftharpoons} S E_{NS,n} \qquad \theta_b \approx \frac{E_T^{n_H}}{K_{D,app}^{n_H} + E_T^{n_H}}$$

B

$$S_f + E_f \overset{K_{D,app1}}{\rightleftharpoons} E_S S + n\,E_f \overset{K_{D,app2}}{\rightleftharpoons} E_S S E_{NS,n} \qquad \theta_b \approx \frac{E_T \bullet \left(K_{D,app2}^{n_H} + E_T^{n_H}\right)}{K_{D,app1} + E_T \bullet \left(K_{D,app2}^{n_H} + E_T^{n_H}\right)}$$

C

$$\begin{array}{ccccccccc} S_f & \rightleftharpoons & S^{i}E_{NS,1} & \rightleftharpoons & S^{i,j}E_{NS,2} & \rightleftharpoons & \cdots & \rightleftharpoons & S^{i,j,k,\ldots}E_{NS,n} \\ \updownarrow & +E_f & \updownarrow & +E_f & \updownarrow & +E_f & & +E_f & \updownarrow \\ E_S S & \rightleftharpoons & E_S S^{i}E_{NS,1} & \rightleftharpoons & E_S S^{i,j}E_{NS,2} & \rightleftharpoons & \cdots & \rightleftharpoons & E_S S^{i,j,k,\ldots}E_{NS,n} \end{array}$$

Figure S11: Stopped flow assessment of binding kinetics. (A) Experimental set-up, as described in the corresponding SI Appendix Methods. **(B)** Stopped-flow traces of Fl-CDC8 rapidly mixed with 0, 20 and 750 nM of D256A Pus7 protein. **(C)** Traces at higher D256A concentrations were biphasic. This shows a 750 nM trace fit with one or two phases. **(D)** All of the $k_{obs,1}$ values measured are plotted as a function of D256A Pus7 concentration.

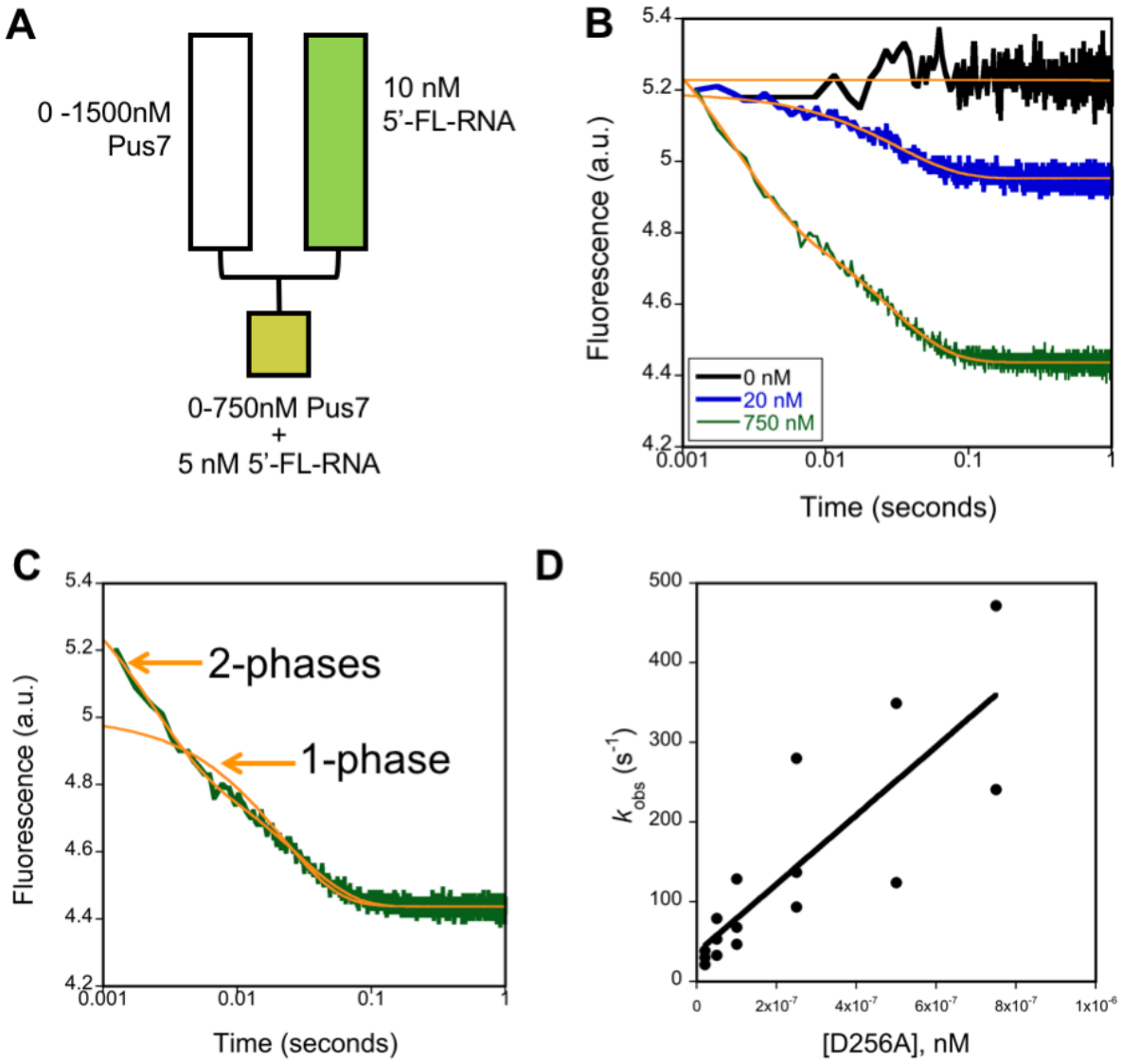

Figure S12: Deletion of ID1 does not broadly affect pseudouridinylation of total RNA in vitro. Total cellular RNA extracted from Δpus7::kanMX was pseudouridinylated in vitro using PUS7FL or PUS7ΔID1. Pseudouridinylation of known sites was assayed using CLAP (25).

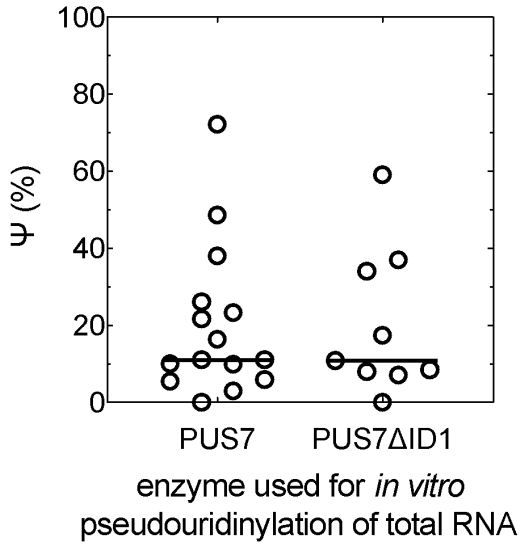

Figure S13: Deletion of ID-I influences pseudouridylation efficiency in a target dependent manner.

Total cellular RNA was extracted from *pus7::kanMX* yeast and pseudouridinylated in vitro with PUS7fl or PUS7ΔID1 (left side) or extracted from *pus7::kanMX* yeast expressing PUS7FL or PUS7ΔID1 (right side). Pseudouridinylation was assayed at specific sites using CLAP (25). The difference between mean pseudouridinylation level at sites in RNA exposed to PUS7ΔID1 and RNA exposed to PUS7fl is shown on the y axis.

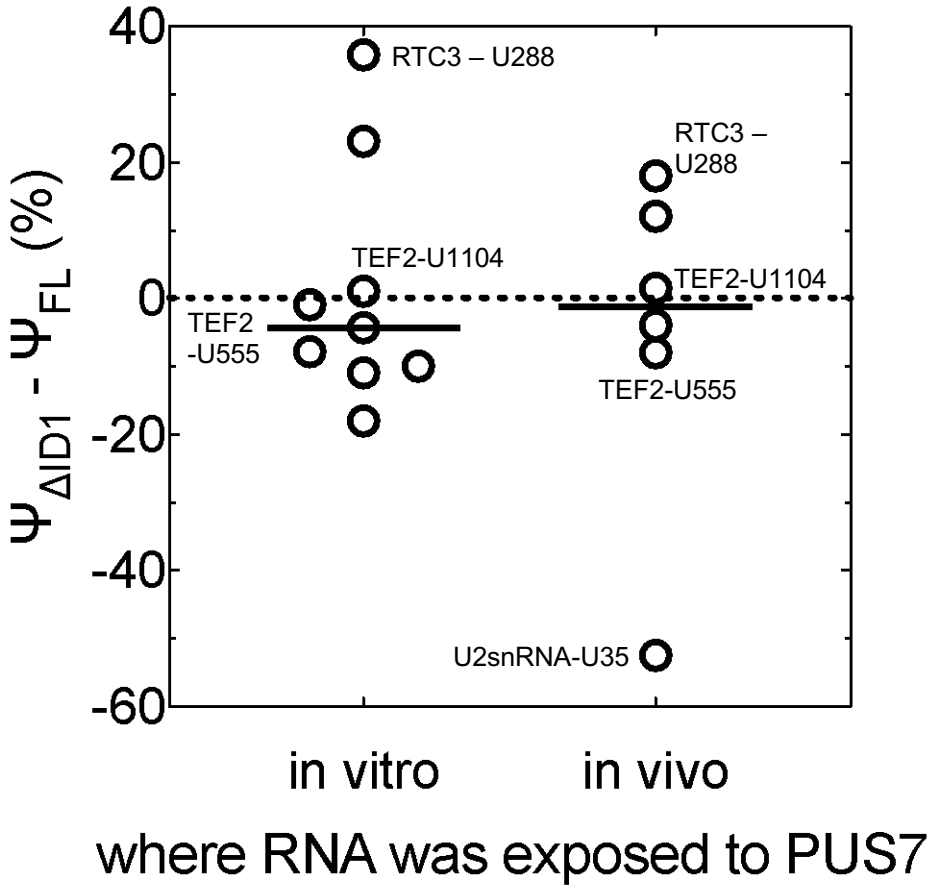

Figure S14: Expression of PUS7ΔID1 confers no obvious phenotypic defects relative to PUS7FL. PUS7 was expressed from a CEN plasmid under the control of a GPD promoter in WT and *Δpus7::kanMX* yeast and assayed by spot plating under the indicated conditions. Three independent transformants were assayed for each plasmid.

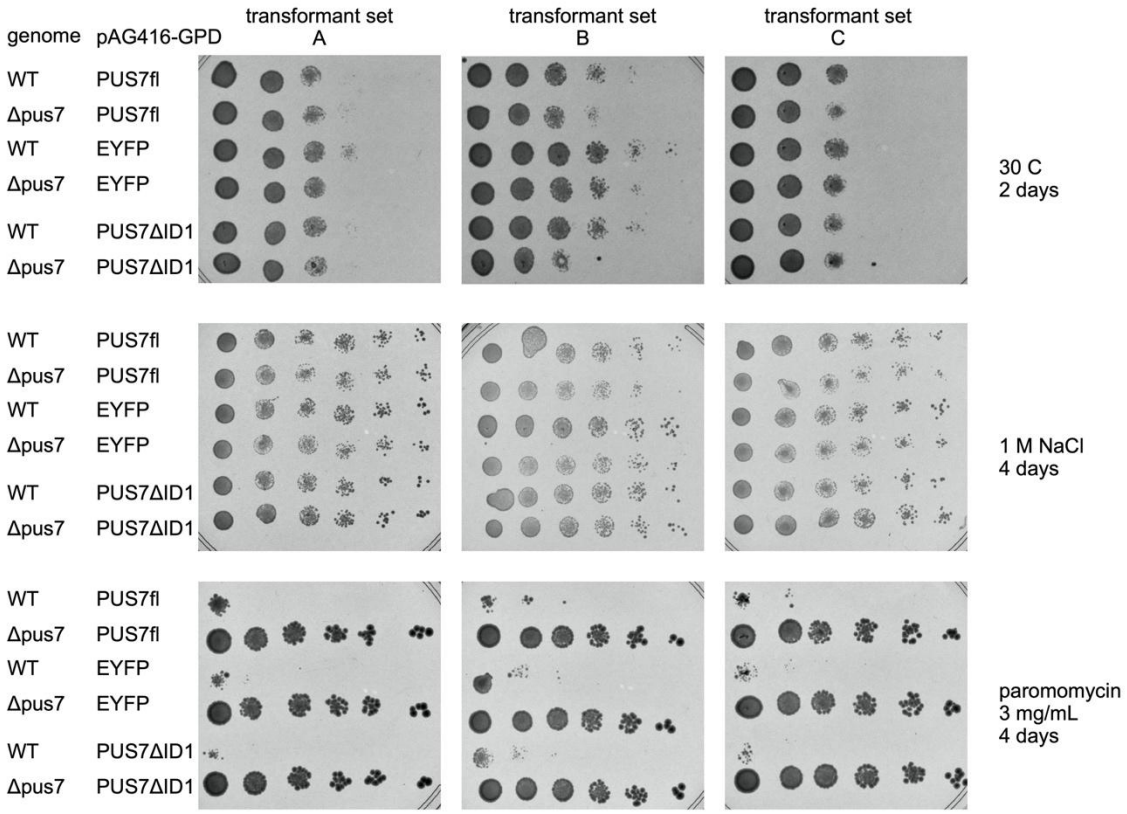

Figure S15: Isolation of PUS7fl and PUS7ΔID1 expressing clones. Three independent transformants were isolated for each strain/plasmid combination.

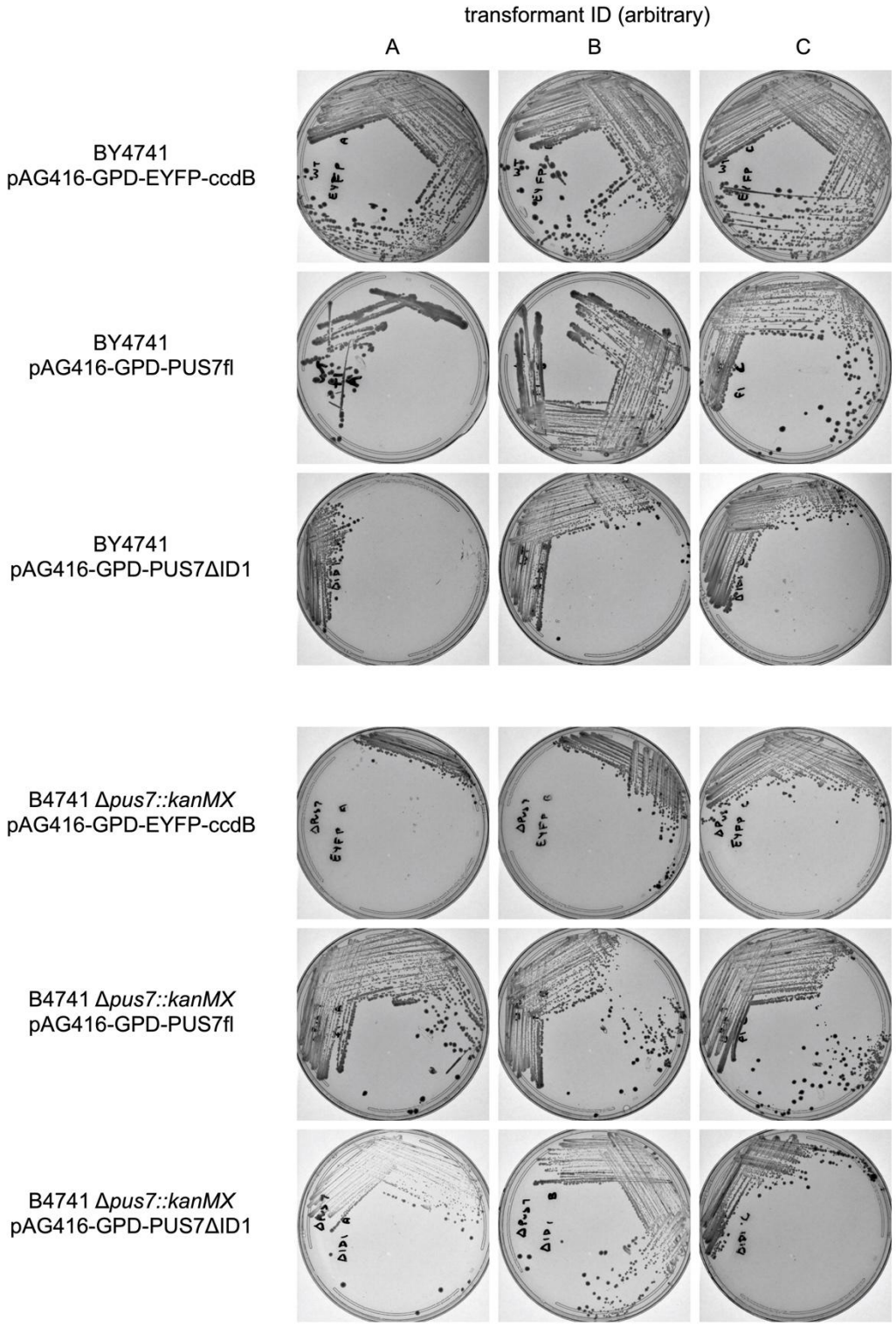

Figure S16: Secondary structure prediction of Pus7 modified sites in mRNA coding regions reported in Carlile, et al. Nature (2014) (23).

YKL103C

Target UGUAG

GCACAGGAAUUCAUUGAUUUCAUUUACAAGAACC
CUACCACUUACCA**UGUAG**UAUCAUUUUUCGCGG
AGCUGUUAGAUAAGCAUAACUUCAAAUACUU

Non-target UGUAG

GUAUUGGUAAACACUUCCUUUUUGCACCACGUCU
AGAUGACAGGUUG**UGUAG**UUUCGCAGCAAUGAUU
GCUUUGAUUUGCUACGCUAAGGAUGUUAAUA

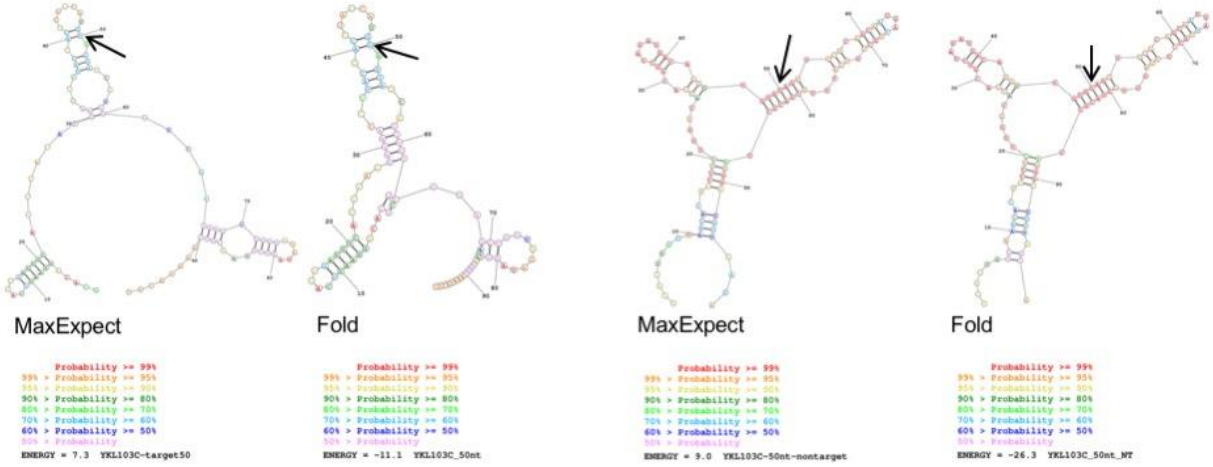

YER069W

Target UGUAG

CAUGGUGUAGUUAUUGGUGGUUUCAAGCUGAAU
GAUGCUGAAGAUCG**UGUAG**UUGUUUGCGCAACC
AUCGAUAACUUACUUAAAGGCGCCGCUACUCAA

Non-target UGUAG

GUCAUCGAUGAUAUCCCACUGGUUAAAGAUAUUG
AGGGCACCCAUGG**UGUAG**UUAUUGGUGGUUUCAA
GCUGAAUGAUGCUGAAGAUCGUGUAGUUGUU

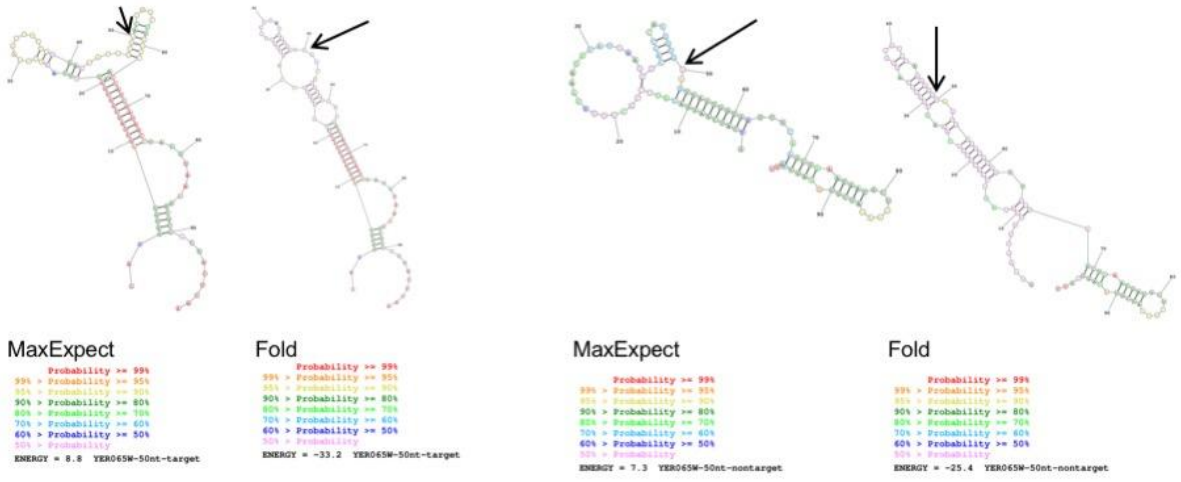

YMR062C

Target UGUAG

UCGAAAAAAGUCCUUGAAACUGCUCGUGGUAAAA
AUAUUAACGCUAU**UGUAG**UCAAUUCCGGUUGUG
CUAACUCAGUCACAGGUGAUCUUGGUAUGAAA

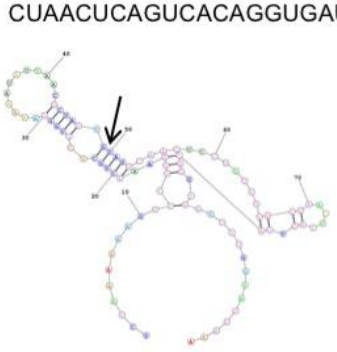

MaxExpect

Fold

YPR176C

Target UGUAG

GCACUAUCAAUUUUGGGUGAAUUAACGUCUGAA
GUUGUUGACCCUGC**UGUAG**ACUUUGUACUCAAG
UGUUAUAAUUUUGAUGGUGGCUUUGGAUUAUGU

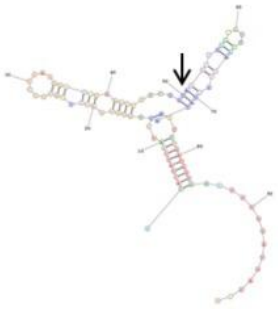

MaxExpect

Fold

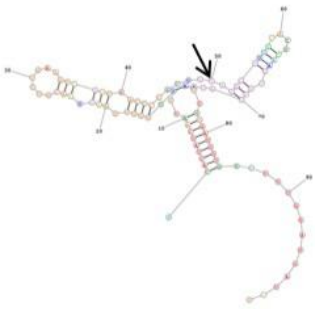

YNL336W

Target UGUAG

AUGAAAGAGAAUGAACUUAAAAAUGAGAAGAG**UG**
UAGAUGUAUUAUCCUUCAAACAGCUCGAAUCCC
AAAAGAUUGUUCUACCUCAAGAUCUUUUCAGA

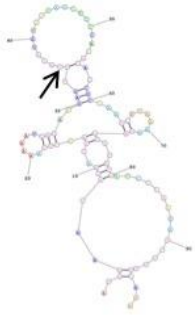

MaxExpect

Fold

YBR032C

Target UGUAG

AUGAAAGAGAAUGAACUUAAAAAUGAGAAGAG**UG**
UAGAUGUAUUAUCCUUCAAACAGCUCGAAUCCC
AAAAGAUUGUUCUACCUCAAGAUCUUUUCAGA

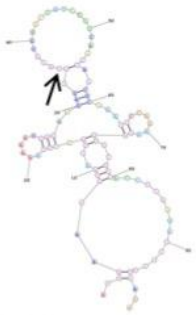

MaxExpect

Fold

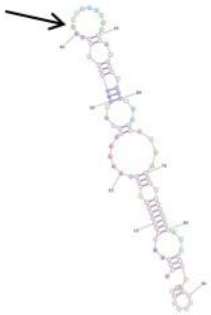

YDR380W

Target UGUAG

UCUAUUCACCUAGUGUUGAAUCAGCUGGCCUAA
GAUGGGUCGGCACG**UGUAA**UGAACUGAACGCCG
CUUAUGCGGCCGACGGAUAUUCCCGUUACUCUA

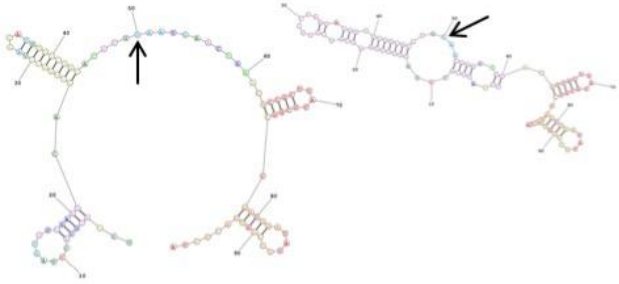

MaxExpect

Fold

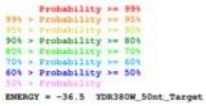

Non-Target UGUAA-1

AUCUGCAAAACUGGGAUUUGGAAUUUUUCCACU
GUUAUGGGAAAAUC**UGUAA**UUGAUGAGUCAAAC
CCAACUUAUAUGGGUCAAUAUAAUGGUAAAGAA

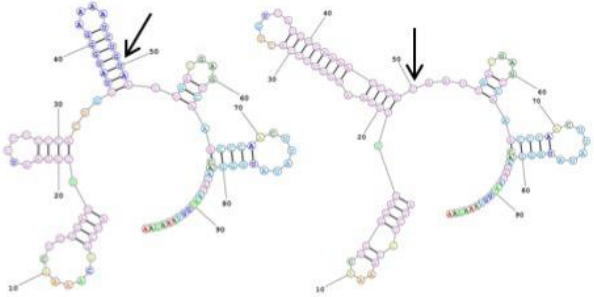

MaxExpect

Fold

Non-Target UGUAA-2

UACAAGCGCAUUGACGUUUCUAAACUUUCUUUG
CAAUAUGAUUCAAA**UGUAA**CUCAAUAUACGAACG
AAACAAUGCGGUUAGAAGAUCCUACCAAUGGA

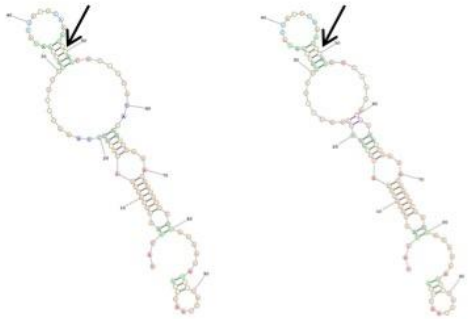

MaxExpect

Fold

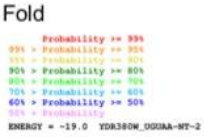

YNR028W

Target UUUAG

AUGAAGAGCUUUUUUCUUUAUCUUUAUGUGGCA
UUCAUG**UUUAG**UUGCAUAACGGCUCUGCCAUUA
CCUGUGGAUAACAAAAGGGCUUCUUCAGACUCC

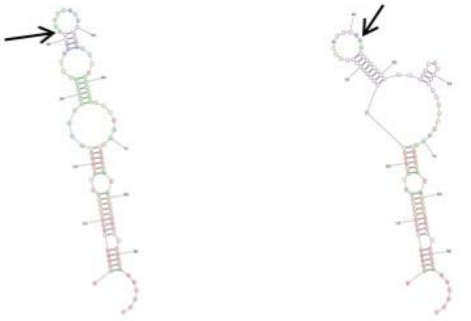

MaxExpect

Fold

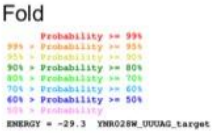

YML132W

Target UGUAG

AUGAAAGAGAAUGAACUUAAAAAUGAGAAGAG**UG**
UAGAUGUAUUAUCCUUCAAACAGCUCGAAUCCC
AAAAGAUUGUUCUACCUCAAGAUCUUUUCAGA

Non-Target UGUAG

UCUGCGAAGAAAUCUAUGUGGCCUUUACCAUUG
AAUGUGGAACUAUGGCCAUACAUUAAAGAAGCG
CAAUUAUCCCGCAGUGAGGUGCUCUUAG**UGUAG**

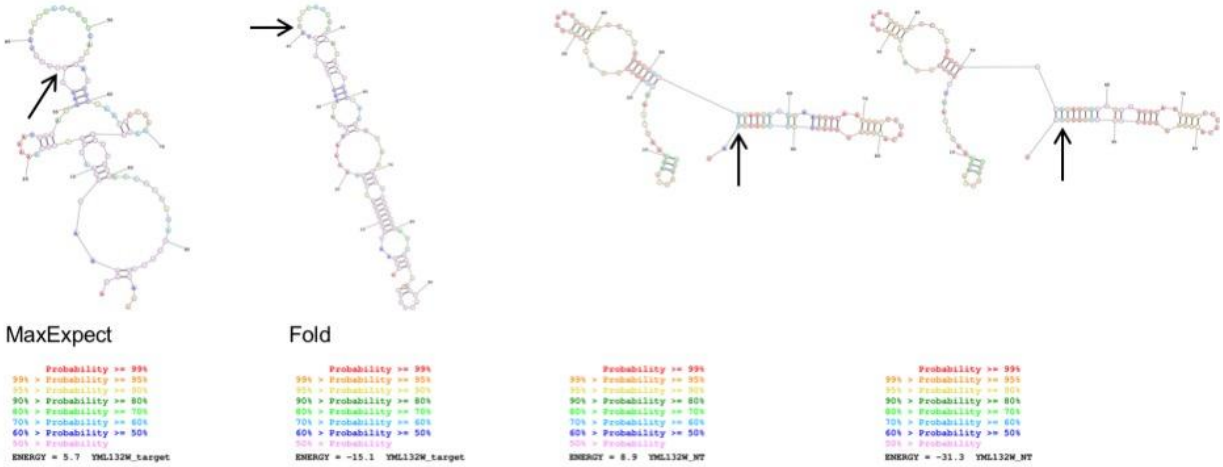

YJR161C

Target UGUAG

AUGAAAGAGAAUGAACUUAAAAAUGAGAAGAG**UG**
UAGAUGUAUUAUCCUUCAAACAGCUCGAAUCCC
AAAAGAUUGUUCUACCUCAAGAUCUUUUCAGA

YBR036C

Target UGUAA

AUGUCUACCACACUACUUUGGUUUUCAAG**UGUA**
AUAGGCUACGUGAUUCAAACAAAAUGUUUGUCU
AACAUACAAUCUAAAAAGGAAAUCUCCGUGGGG

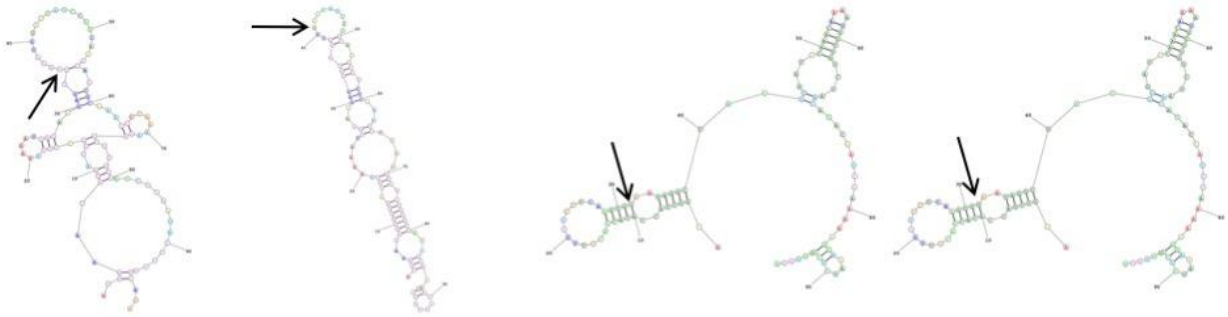

YPR124W

Target AUUAU

CAGUAGCUCUUCAGGGAUGGAUAUGGACAUGAG
UAUGGGAAUGAACU**AUUAU**CUGACUCCCACAUA
UAAAAACUAUCCAGUUUUGUUUCACCAUUUGCA

MaxExpect

Fold

Non-Target AUUAU - 1

AUGGCGUCGAUGAGCAUGGAUGCGAUGUCUAGU
GCCAGCAAAACGAU**AUUAU**CGAGCAUGUCAUCG
AUGAGCAUGGAAGCGAUGUCCAGUGCGAGCAAA

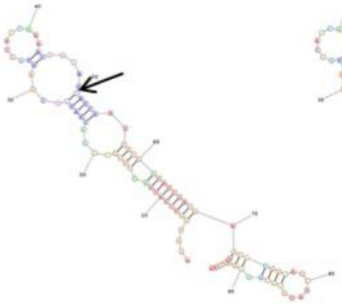

MaxExpect

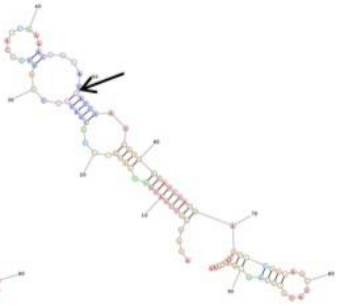

Fold

Non-Target AUUAU - 2

UAAAUAUUCCACUUUACCUUCAGCAAACUCCAAA
GACGAAGGAAAAC**AUUAU**GACACAGAGAAUAAUU
UUGAAAUUCAAGGUUUACCUAAGCUGCCAAA

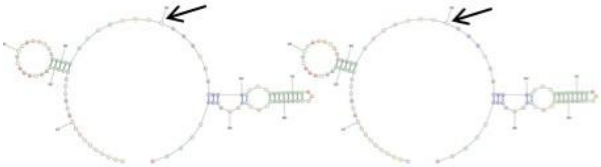

MaxExpect

Fold

Non-Target AUUAU – 3 & 4

UAUUUGUUCCAUCUUUAAUGGAUCUCUUUCAUG
AC**AUUAU**AAGGGCGUUCUUAGUAUUUACCUCUA
CGAUG**AUUAU**UUAUAUGUUGAUGCUUGCUACCA

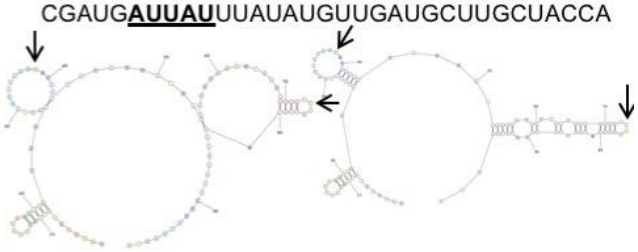

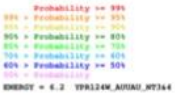

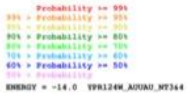

YDR152W

Target UGUAG

GGCGUGGUGGGCACAGGCGACGAGUAUAUGGAA
GAGGAUGACGCGAG**UGUAG**AUGACGUAGCCAAG
GGACUUGCCAAGACCGAAAUAGCAAAUCAAUAA

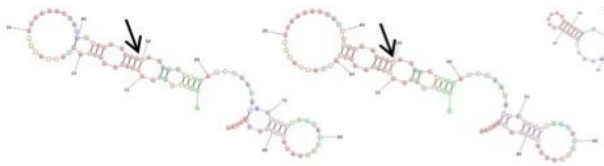

MaxExpect

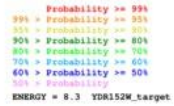

Fold

YLR258W

Target UGUAG

UGGUUGGCCGGUGUUGCGUUACCAUUAUGCCG
UAAAAGGCGUAUCGA**UGUAG**UUACCAUUtgtUUCA
CCACUCAUGCUACUUUAUUGGGACGGUAUUUA

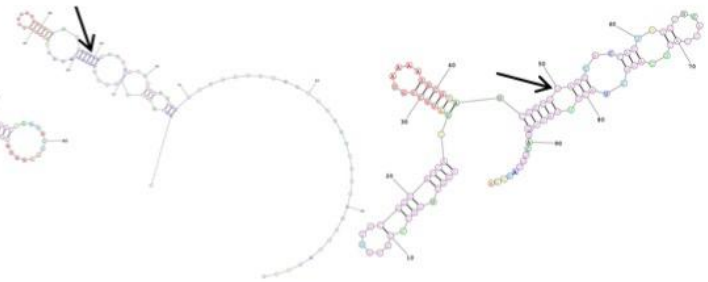

MaxExpect

Fold

YCL026B-C

Target UGUAA

GCCGGUCAAAAGAGGCCUGCUUCAGCAAGGGAU
GAGGCCUUUGGUUC**UGUAA**UCUUCUUCACCGAC
GACAAGGUAACUGAAAAGCUAAAGGCUGACUUC

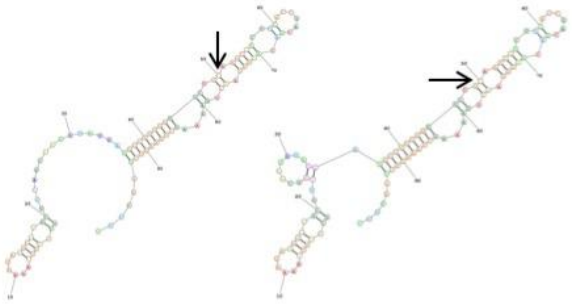

MaxExpect

Fold

YDR497C

Target UGUAG

AAGACAUCGCAAUCAAAUGUUGGUGAUGCCGUU
GGCAACGCUGAUAG**UGUAG**AGUUCAACAGUGAG
CAUGACUCACCUUCAAAGAGAGGUAAAAUUACA

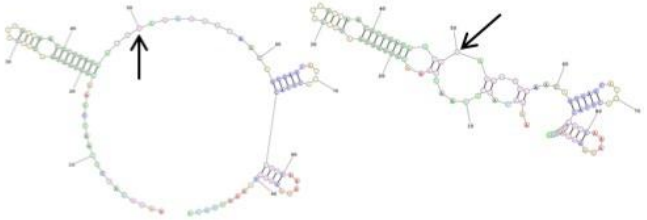

MaxExpect

Fold

YNL117W

Target UGUAG

AUUAUCGUGAGACCCCGUGGUUGGCACAUGGUG
GAAAAGCACCUUUA**UGUAG**AUGAUGAACCAAUCA
GCGCUUCCAUCUUUGAUUUUGGUUUAUAUUUC

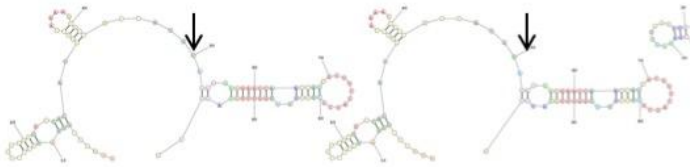

MaxExpect

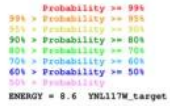

Fold

Non-Target UGUAG

AAGAUGGAGCACCACUUGGAAGCUAAACUAUGG
AACGACGUCUUCUG**UGUAG**CUCAAGAUUACAUU
GGGAUCCCAAGGGGUACAAUCAGAGCUACUGUG

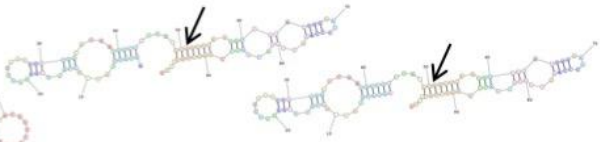

MaxExpect

Fold

YBR122C

Target UGUAG

GCUAUUUAUCACCAAUUCAAUGUCAAAAUGGAGU
UGAGUGAUGGAAG**UGUAG**UUAUCCGGAGAUCCC
AAUAUCCAAAGGGUGAAAUUAGAUUAAUUCAA

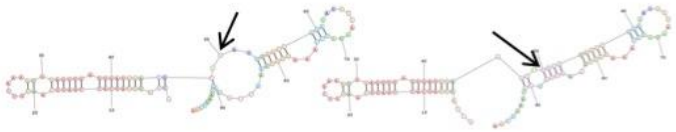

MaxExpect

Fold

YNR036C

Target UGUAA

GCUCCACAACUGGAUCAGUGUCCCCAGCGGAAG
GGUGUCGUAUUACG**UGUAA**UGGUUUUAAAGCCC
AAGAAGCCGAAUUCUGCGCAGAGAAAGGCGUGC

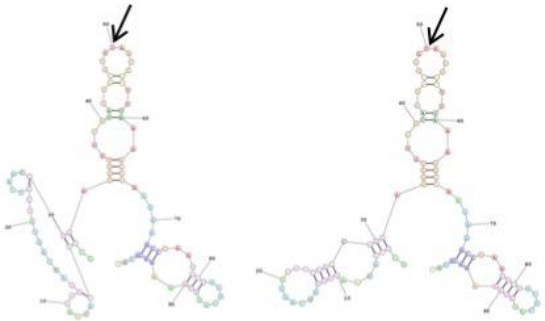

MaxExpect

Fold

YCL043C

Target UGUAG

GAUGAUUUCAAGCUUUCUAUUUACUUGCCCUCC
GCCAUGGACGAGCC**UGUAG**UAUACAACGGUAAG
AAAGCCGAUAUCGCUGACGCUGAUGUUUUUGAA

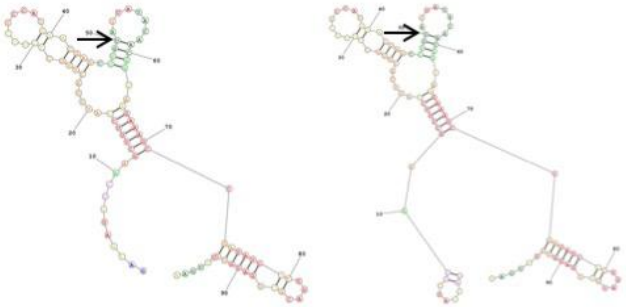

MaxExpect

Fold

YOL038W

Target UGUGU

GGUGUGCAACAAAGGUACACGCAGUCAGGAGGU
GUUAGACCAUUUGG**UGUGU**CGACGCUGAUUGCC
GGCUUCGACCCGAGAGAUGAUGAACCCAAGCUU

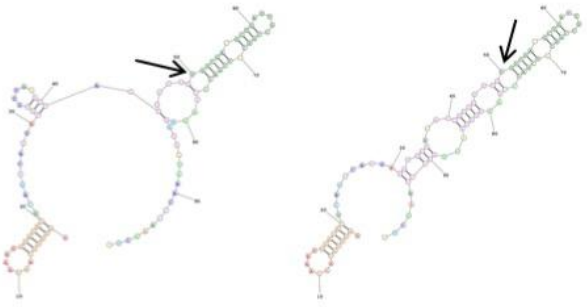

MaxExpect

Fold

Non-target UGUGU -1

AGGCGGUAAAGAGGGGUACCUGUGCUGUAGGUG
UCAAGGGUAAGAAU**UGUGU**AGUAUUGGGCUGCG
AAAGAAGGUCUACUUUGAAGCUGCAAGACACUA

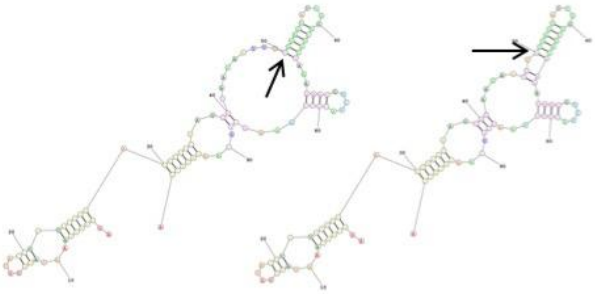

MaxExpect

Fold

Non-target UGUGU - 2

UGGAGAAGAAUUACGAUCGCAAAGAACCACCAGC
CACAGUGGAAGAA**UGUGU**CAAACUUACUGUAAG
AUCUCUGUUGGAGGUAGUUCAAACAGGUGCAA

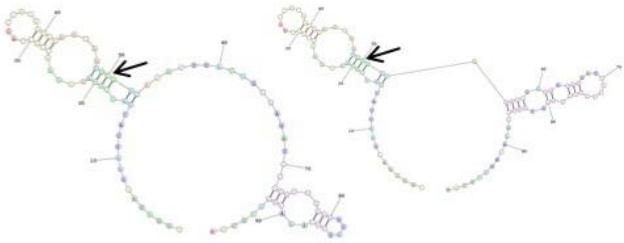

MaxExpect

Fold

YMR308C

Target UGUAG

AUUGAAAAUAAUUCGCCAAUUGUGUGUGCUCAA
UCUAAUAUCUCCGC**UGUAG**UUGAUUCAGUCAUA
CAAGCCUUGAAUGAGAGAAGUUUGACCGAAAGG

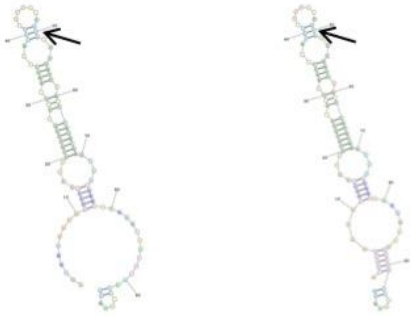

MaxExpect

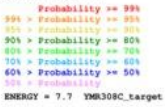

Fold

Non-Target UGUAG

CUUCAGAUUGUCCAGGCGUUUGCUUCCCCUGAC
AAUCAAAUACGUUC**UGUAG**CUGAGAAGGCUCUU
AGUGAAGAAUGGAUUACCGAAAACAAUAUUGAG

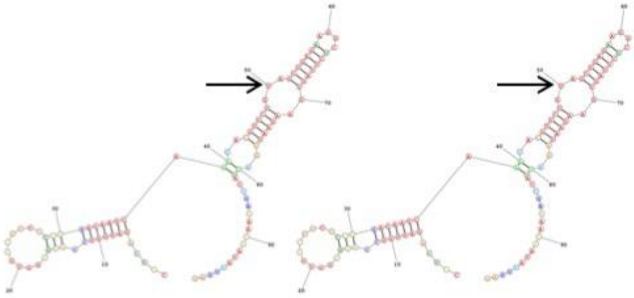

MaxExpect

Fold

YHR141C

Target UGUUA

AUGGGUAUGUGGACGAUUAGGAAUAGACAAACC
A**UGUUA**UUUAUCUCCAUUAGGGCGUGAGAGUGU
AAUUAGUACACAGGUACUACUAGAAUGCUAAAG

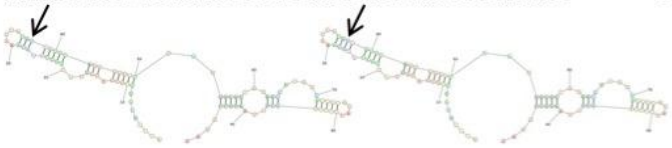

MaxExpect

Fold

YDR322C-A

Target UGUAG

UUGAAGCUGGUAGAGGAGGCAAAGAAGGAAUAC
GCCAAGCUACACCC**UGUAG**UAACUCCUAAAGAU
GUGCCUGCGAACGCCUCAUUUAAUUUGGAAGAU

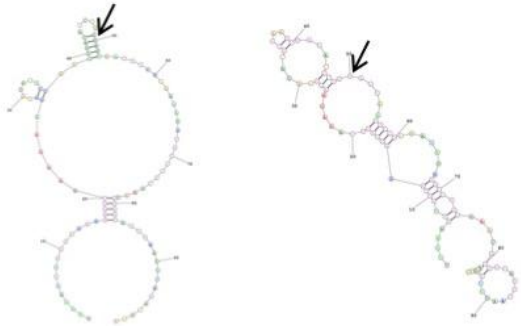

MaxExpect

Fold

YOR305W

Target AGUAG

ACCGGUGGCGCCCAUGAUGGUGGCGUAGACAUA
AAGGGAAGCUGGCC**AGUAG**AUGAUAUUUAUUGG
AAAAUUUCAUCGUUAAUGCCCAAUUUGGAAAUG

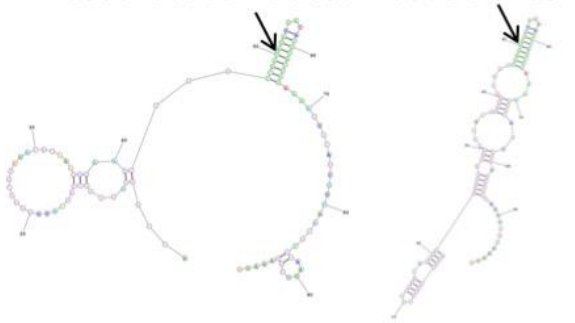

MaxExpect

Fold

Non-Target AGUAG

AAGGCUUUCACUAAAUCAAAAUUAUCUCCUAGAG
AAUUCCGUGAGUU**AGUAG**GAACAUUCACCUCAC
UAGUAUCACAUAGUCAACGCAACAAAACAGUA

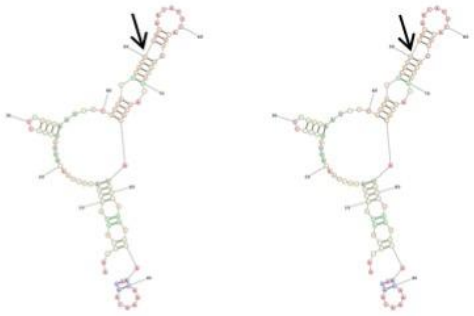

MaxExpect

Fold

YPR198W

Target UGUAG

AGAGUCGUUGCUGGGUUUGGAGGAAGUGGAAUU
GAAUCACUUGCUUU**UGUAG**UUGGAACAUCCAUU
GUCCGAGAAAACCAUAGAGGAAUUAUGAUAACG

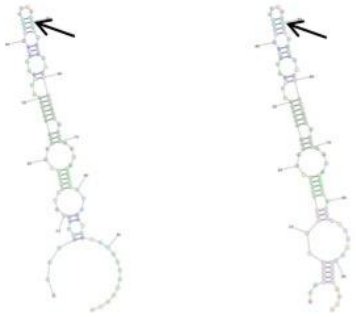

MaxExpect

Fold

Non-Target UGUAG

AAAAACCAGAUGCGCUCUUCCCAAUUAAACAUAC
CACAAUUUACGUC**UGUAG**AAACACUUUUAGCGU
AUAGCACAGAACAUUAUGAUGGCCCCCAAUCU

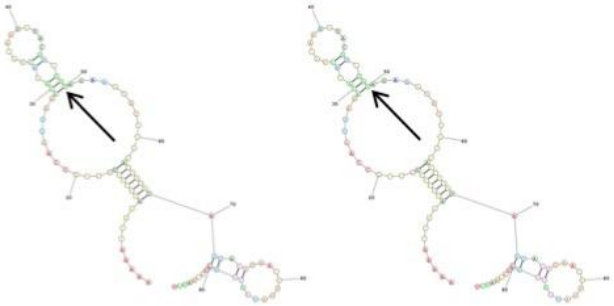

MaxExpect

Fold

YGL115W

Target UGUAG

UCUACUAUUAUGGAUAACAUCAGAAAAGCAAGGG
UGCAUAGAUUCUU**UGUAG**UUGAUGACGUCGGAC
GGUUGGUUGGUGUCUUGACGUUAAGCGAUAUU

Non-Target UGUAG

CCGACACAGGAUUCACAAGAAAAGGUUUCUAUU
GAACAGCAGUUAGC**UGUAG**AAUCGAUAAGGAAG
UUUUUGAACUCGAAAACAUCUUAUGACGUGUUG

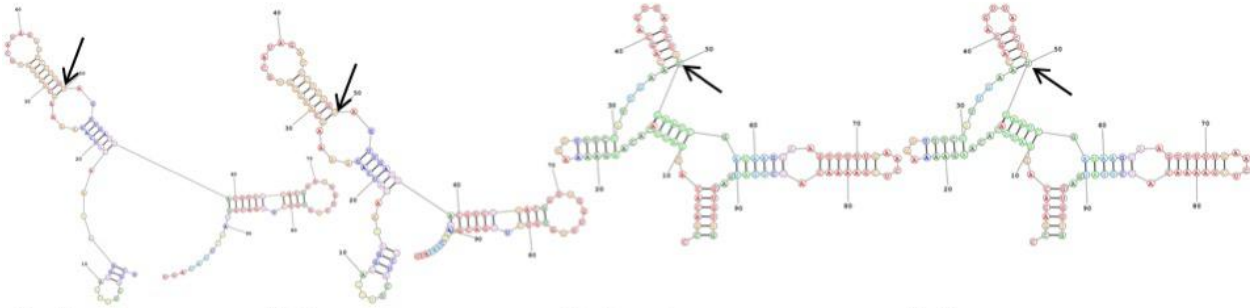

MaxExpect

Fold

MaxExpect

Fold

YPR009W

Target UGUAA

AUGAAGCCGAACAAUCGAACUUGUGA**UGUAA**UU
ACCAACAAAGAUGAAUCUCUUCCUGCACUUUUG
CUGCCUGCACUGAACAGUUACACCUGUGACGAU

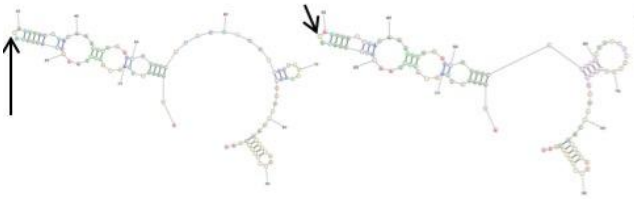

MaxExpect

Fold

YER150W

Target UGUAA

GCCAUGGCCUCUACGGCUCUCGGAUUGGUAUCU
AAUUCUAGUUCCUC**UGUAA**UCGUGGUACCAUCA
AGCGAUGCUACUAUUGCCGGUAACGAUACAGCC

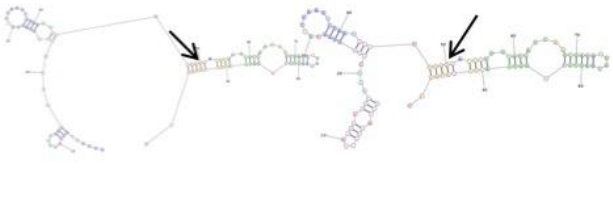

MaxExpect

Fold

YLR354C

Target UGUAA

AAGGUAUUCAAGCUGCCAAAGAAUUGGAAGAAAA
GGACGGUAUCCAC**UGUAA**UUUGACUCUAUUAUU
CUCCUUCGUUCAAGCAGUUGCCUGUGCCGAGG

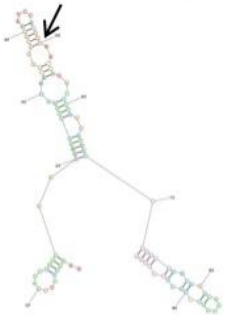

MaxExpect

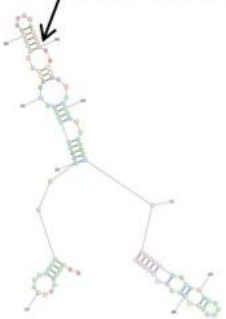

Fold

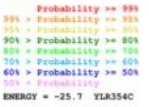

YPL230W

Target UGUAG

ACUGCAGGCGUUCUUACGAGCAGCAAUGGUAAC
UUUGCCACCAAUAG**UGUAG**CGGCAUCAACUCCG
AAGAGGUCCAAAAGUGCUCGAAGGAAAACGUUC

MaxExpect

Fold

YHR140W

Target UGUAG

ACCGCGUGUCUUUUGACGAGCACCUGGGGGUUU
GUUAGGGCCACAUC**UGUAG**UCUUACCUCCAAGU
UUAAGUAAAGCAGGCCAUAAACAGUUUCUAACC

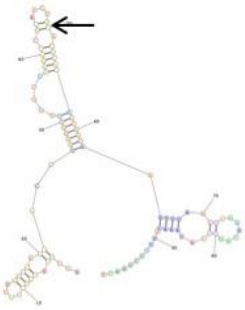

MaxExpect

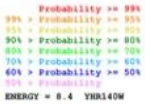

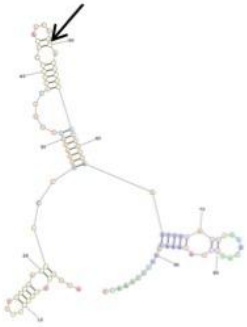

Fold

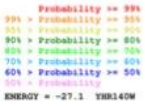

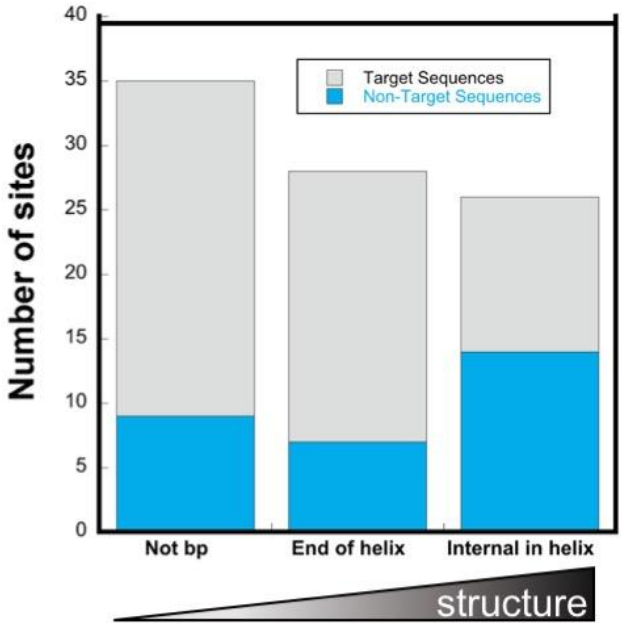

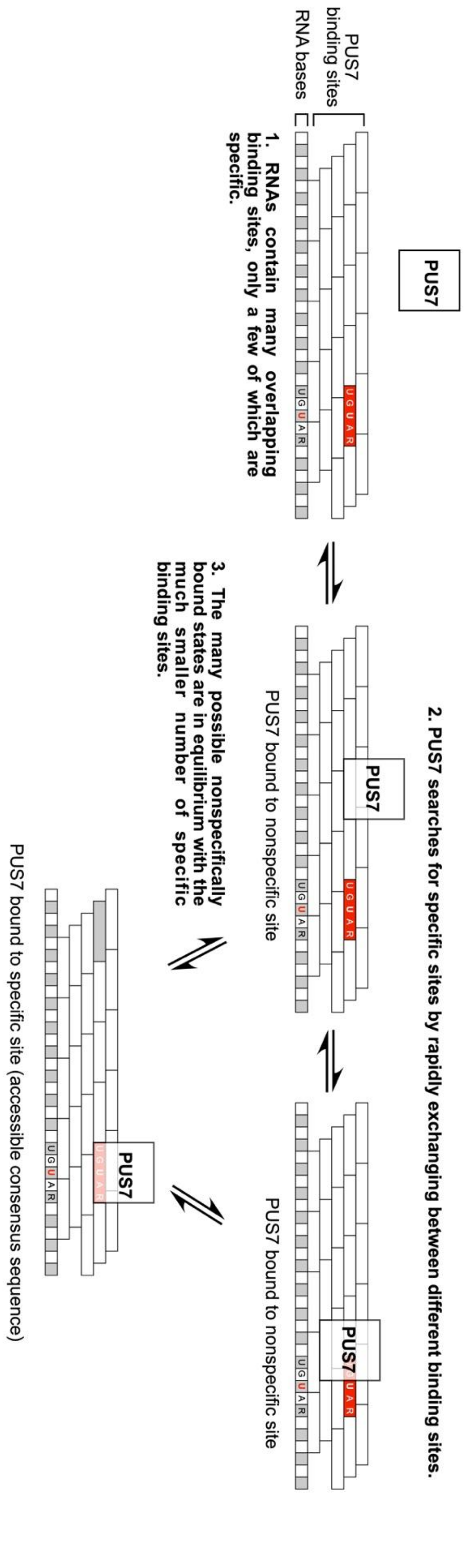

Figure S17: Model - Pus7 rapidly samples RNAs for specific modifiable sequences. RNAs contain multiple (often overlapping) potential Pus7 binding sites. These sites have varying degrees of accessibility to Pus due to their secondary/tertiary structures or occlusion by RNA-binding proteins. Pus7 rapidly samples all accessible sites on a given RNA, forming nonspecific interactions with most sequences. When Pus7 interacts with a modifiable (e.g. UG<u>U</u>AR) sequence, it forms a tighter, 'specific' interaction that results in Ψ installation. Only a handful of the potential Pus7 sites are modifiable and 'specific.'

Figure S18: Secondary structure predictions at 30°C and 45°C of randomly selected Pus7 heat shock targets Schwartz, et al. Cell (2014) (24).

YBL030C

Target UGUAG – 30°C **45°C**

UACAAUGCUCUAAUGAAAAUAUUUUUCAUUGUAU
CUACCGCUUACAU**UGUAG**UGCUAUUACAAGGGU
CUAAAAGAACCAACACCAUUGCGUAUAAUGAA

MaxExpect Fold MaxExpect Fold

YBR103W

Target UGUAG – 30°C **45°C**

CAAGACAAUGAUUAUAUAUUUGAUCUGUCAUGGA
ACUGUGCGGGAAACAAGAUUUC**UGUAG**CAUACU
CGCUUCAAGAAGGUUCAGUUGUAGCCAUAUAA

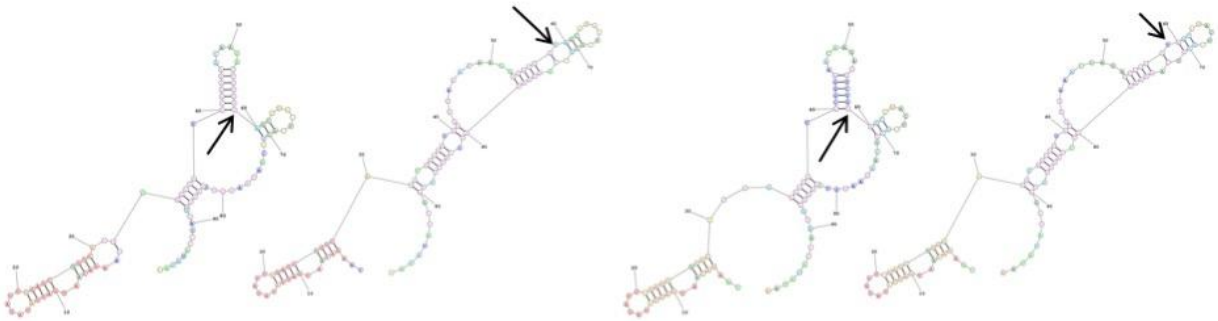

MaxExpect Fold MaxExpect Fold

YBR118W

Target UGUAG – 30°C **45°C**

CUGCUGGUUACUCUCCAGUUUUGGAUUGUCACA
CUGCUCACAUUGCU**UGUAG**AUUCGACGAAUUGU
UGGAAAAGAACGACAGAAGAUCUGGUAAGAAGU

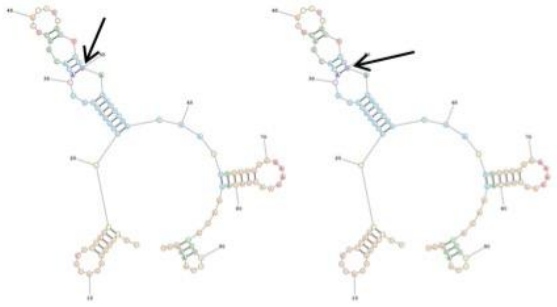

MaxExpect

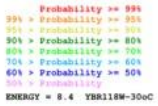

Fold

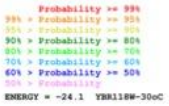

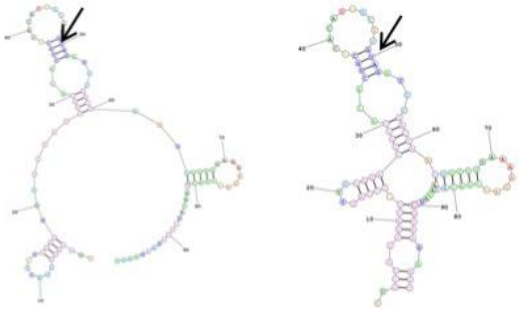

MaxExpect

Fold

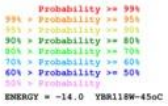

YBR191W

Target UGUAG – 30°C **45°C**

UAGAAAAAAGAUUAAACUUAAGAGUUGAACACAU
CAAGCACUCCAAG**UGUAG**ACAAGAAUUUUUGGAA
AGAGUUAAGGCCAAUGCUGCUAAGCGUGCUG

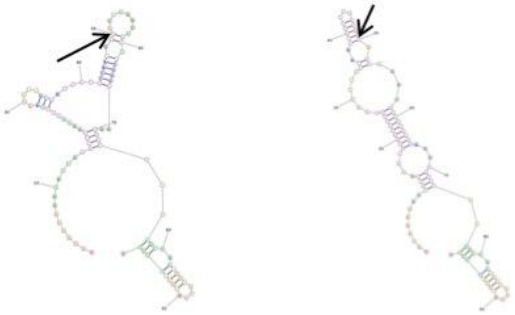

MaxExpect

Fold

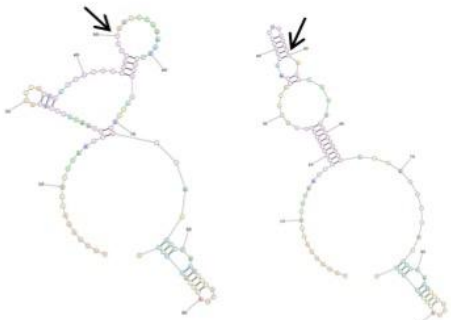

MaxExpect

Fold

YBR252W

Target UGUAG – 30°C **45°C**

GCCCAAUUGAUUCUGGAAAAAAUUGUCGAUGAU
GCCCAGAUCGUUGU**UGUAG**ACUCUCUGGAAGAA
AGUGCAAGAGGGGCCGGUGGCUUUGGUAGCACU

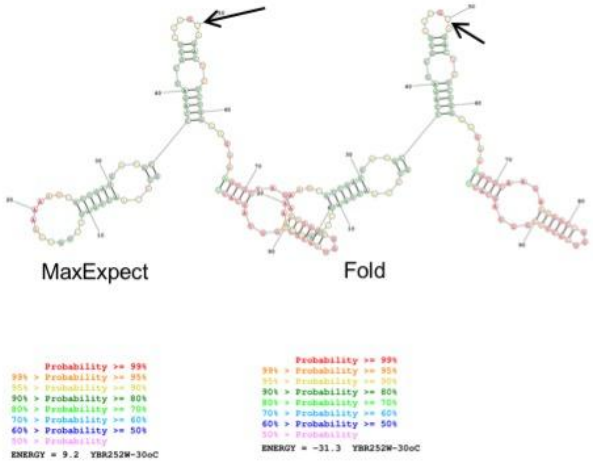

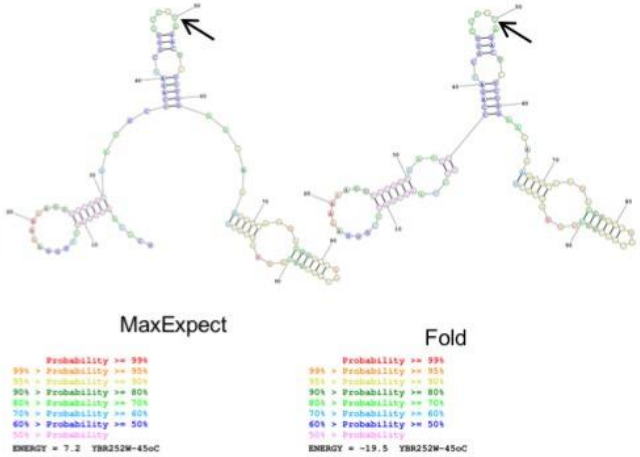

YBR230C

Target UGUAA – 30°C **45°C**

UUGUCUUGGUCAACUUGUUGCUGCAUUCUUCAG
UGGUAUGUUAUUUA**UGUAA**CGGGUAUGCGAACC
ACAACGCCAGAUUCUUGAAGGGGAAACCUAACU

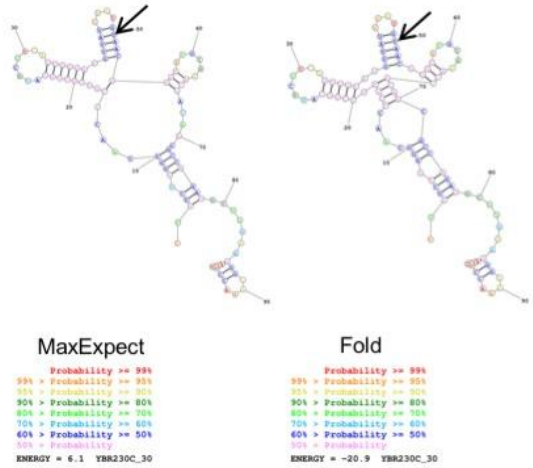

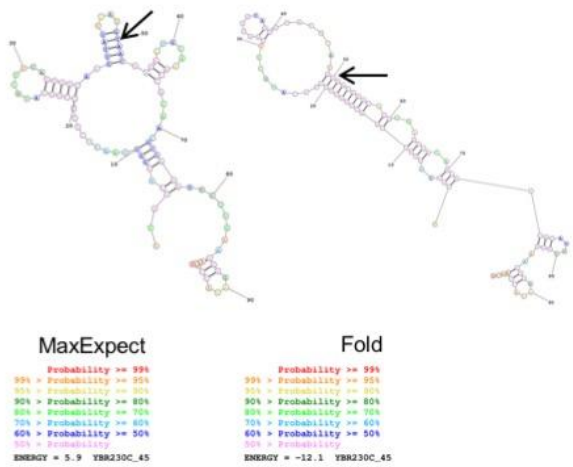

YDL022W – U403

Target UGUAG – 30°C **45°C**

UCGACAUCAUCGUUUUCAACAUUCCACAUCAAUU
UUUGCCCCGUAUC**UGUAG**CCAAUUGAAAGGUCA
UGUUGAUUCACACGUCAGAGCUAUCUCCUGUC

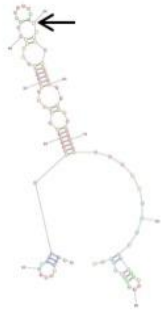

MaxExpect

Fold

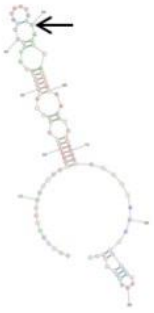

MaxExpect

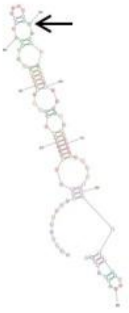

Fold

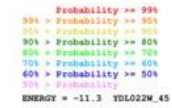

YDL022W – U172

Target UGUAA – 30°C **45°C**

GAUCUGGUAACUGGGGUACUACUAUUGCCAAGG
UGGUUGCCGAAAAU**UGUAA**GGGAUACCCAGAAG
UUUUCGCUCCAAUAGUACAAAUGUGGGUGUUCG

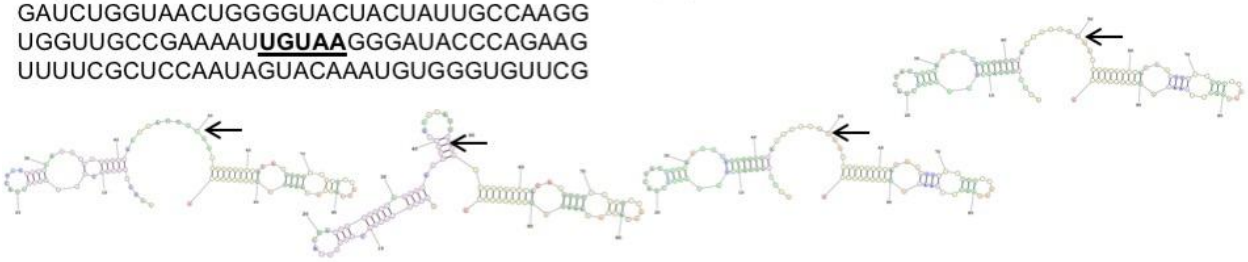

MaxExpect

MaxExpect

Fold

YDL084W

Target UGUAA – 30°C **45°C**

AAGUCAUGAUGUUUUCAGCCACACUUUCUCAAGA
AAUUAGACCAAUU**UGUAG**ACGCUUCUUACAGAAU
CCAUUGGAAAUUUUCGUCGAUGAUGAAGCUA

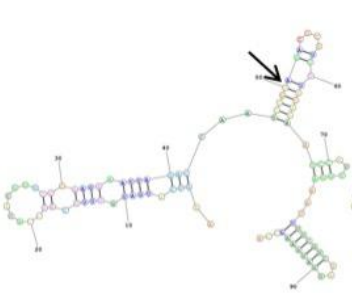

MaxExpect

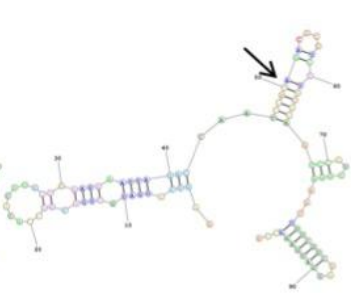

Fold

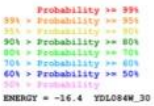

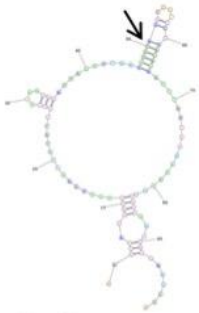

MaxExpect

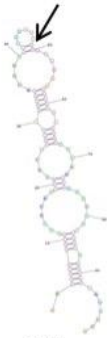

Fold

YDR037W

Target UGUAA – 30°C **45°C**

AAAAGGAUCAAGGUGAUGACGAAGCUCAAUUAGU
CGAUGAAACCUUC**UGUAA**UGCUCUAGAAUACGG
UUUACCACCAACUGGUGGUUGGGGUUGUGGUA

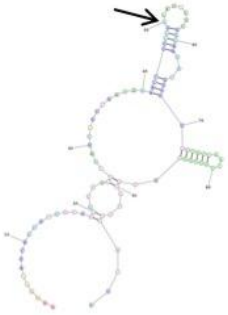

MaxExpect

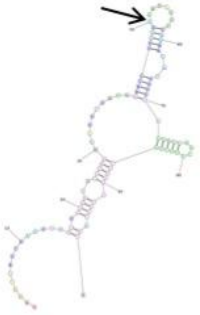

Fold

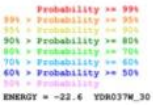

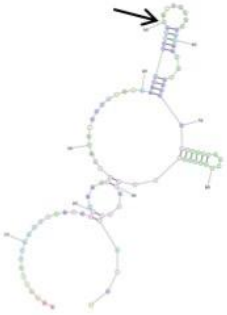

MaxExpect

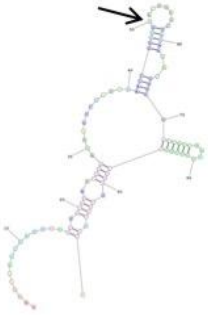

Fold

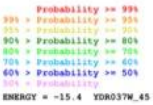

YDR077W

Target UGUAG – 30°C **45°C**

ACCACUCCUCCUUACAACCCAUCUACUGACUACA
CCACUGACUACAC**UGUAG**UCACUGAAUAUACUAC
UUACUGUCCAGAACCAACCACUUUCACCACA

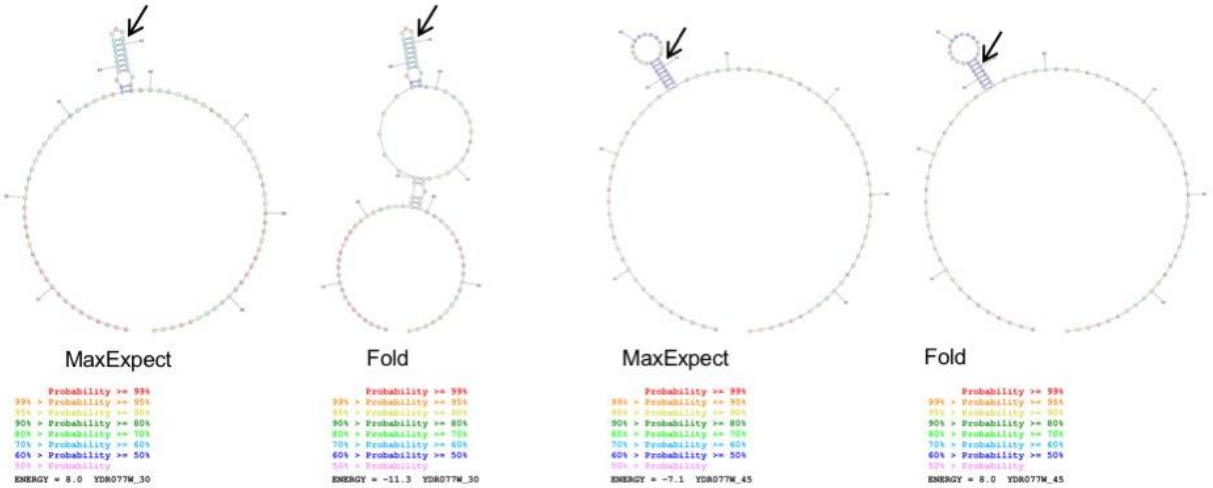

YFL038C

Target UGUAG – 30°C **45°C**

ACCAACGACUACAUCUCCACAAUUGGAGUGGACU
UCAAGAUUAAGAC**UGUAG**AACUGGACGGCAAGA
CUGUAAAGCUACAGAUUUGGGACACUGCAGGU

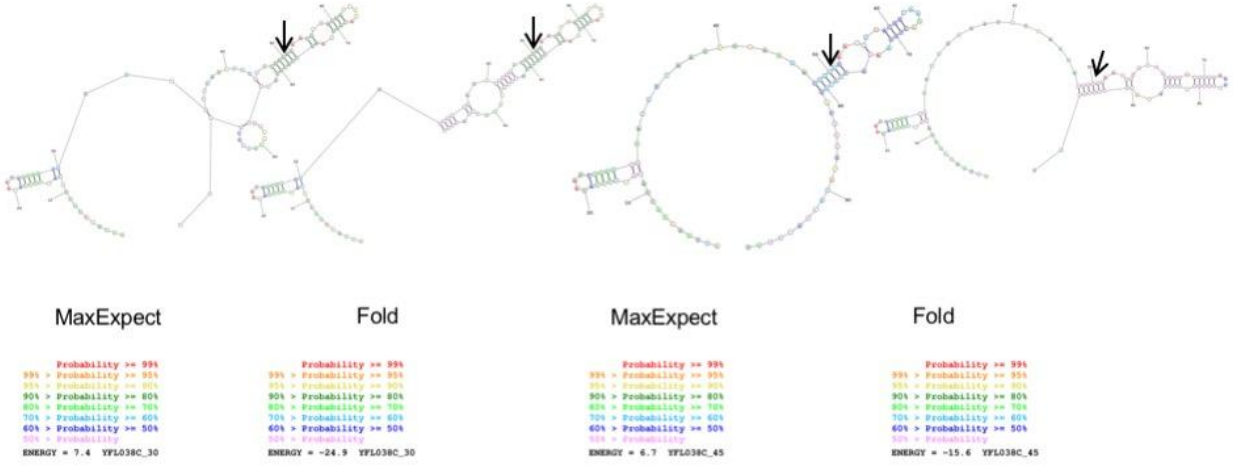

YGL116W

Target UGUAG – 30°C **45°C**

AUUGCAGAUCUGGACGUUCUUUUGGGCCUAAAU
GGUCGCUCGUCGGA**UGUAG**ACAUGACAACCACA
UUGCCGAGUUUGAAGCCACCUCUGCAAAACGGA

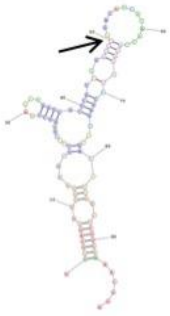

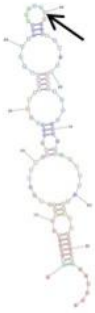

MaxExpect

Fold

MaxExpect

Fold

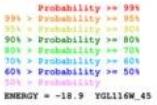

YIL076W

Target UGUAG – 30°C **45°C**

ACGGCUCAAGCUAUCUUGGGUGACUUAGAUAAA
AGUUUGGAGACAUG**UGUAG**AAGGGAUUGACAAU
GACGAAGCAGAAGGGACUACAGAAUUAUUGCUG

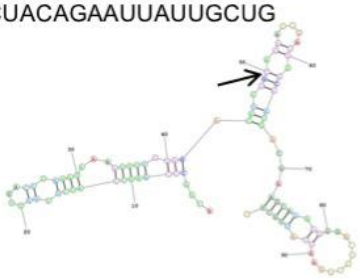

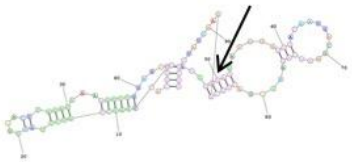

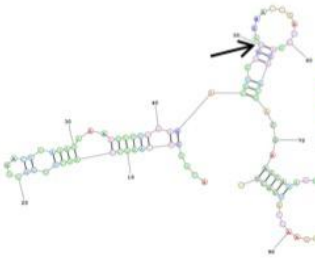

Fold

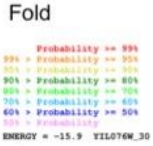

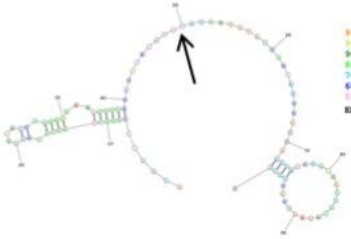

Fold

MaxExpect

MaxExpect

YJL158C

Target UGUAG – 30°C **45°C**

CAAUGUCUAUCCGGCAAUUUCUACAACUUGUAU
GAUCAAAACGUCGCCGAACAA**UGUAG**UGCCAUU
CAUUUGGAAGCUGUUUCUUUGGUCGACUGUUAA

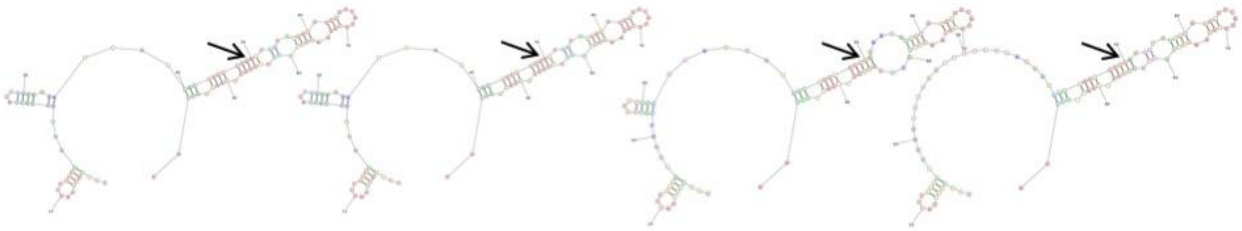

MaxExpect Fold MaxExpect Fold

YLR168C

Target UGUAG – 30°C **45°C**

UCCAGCAGGAAGCCCAAAUUACAGCAUAUGGAUC
CAUUAGAAAGCUG**UGUAA**UAAGAUGGAAGAUUG
GUCAGUUCAAAGGUUUUGCGAGAACGCUAAAA

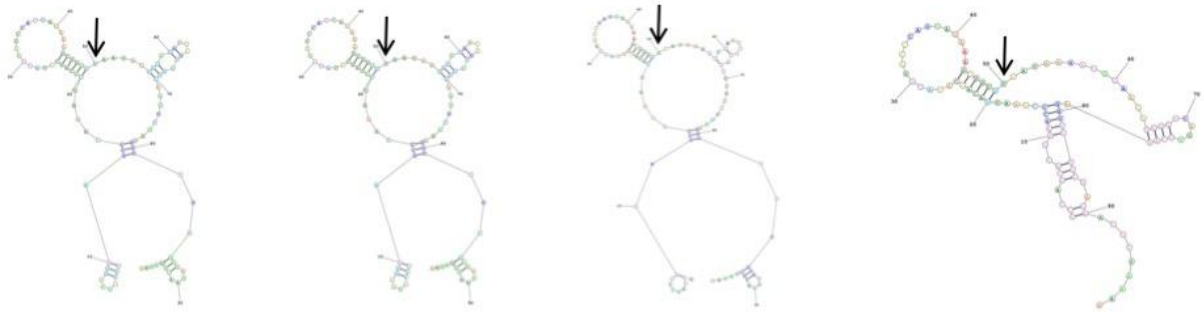

MaxExpect Fold MaxExpect Fold

YLR259C

Target UGUAG – 30°C **45°C**

CCUUUAUUGCGUCGUGCUUACUCCUCUCAUAAA
GAAUUGAAAUUCGG**UGUAG**AAGGAAGAGCCUCC
CUUCUUAAGGGUGUCGAAACUUUAGCUGAAGCG

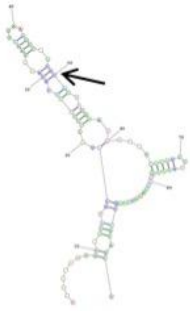

MaxExpect

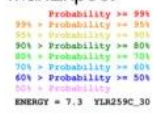

Fold

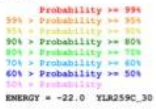

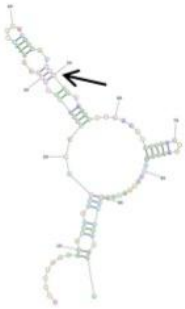

MaxExpect

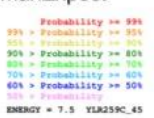

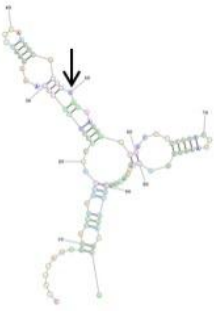

Fold

YMR083C

Target UGUAG – 30°C **45°C**

CCAUUACCUGUUAAACUACCAUUAGUAGGUGGU
CAUGAAGGUGCUGG**UGUAG**UUGUCAAACUAGGU
UCCAAUGUCAAGGGCUGGAAAGUCGGUGAUUUA

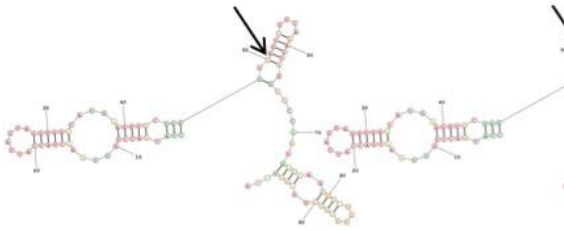

MaxExpect

Fold

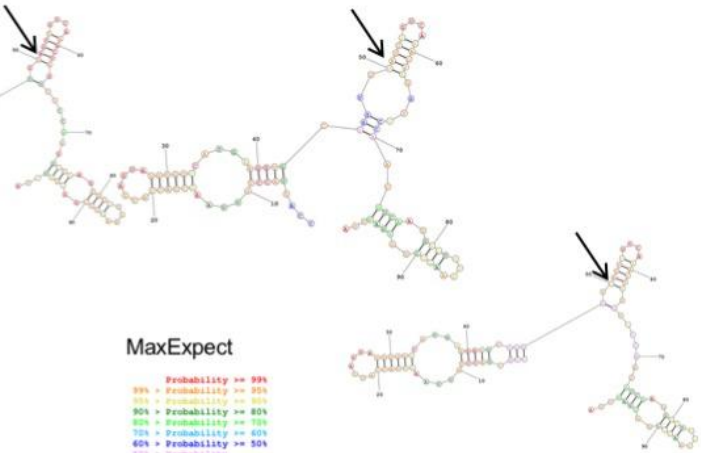

MaxExpect

Fold

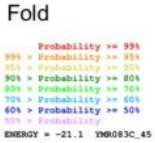

YMR226C

Target UGUAG – 30°C **45°C**

GACGUGGCUGAUCUGAUCGUCUAUGCAACUUCC
AGAAAACAAAAUAC**UGUAA**UUGCAGACACUUUAA
UCUUUCCAACAAACCAAGCGUCACCUCAUCAU

YNL098C

Target UGUAG – 30°C **45°C**

GGUGUUGGUAAAUCUGCUUUGACCAUACAAUUG
ACCCAAUCGCACUU**UGUAG**AUGAAUACGAUCCCA
CAAUUGAGGAUUCAUACAGGAAGCAAGUGGUG

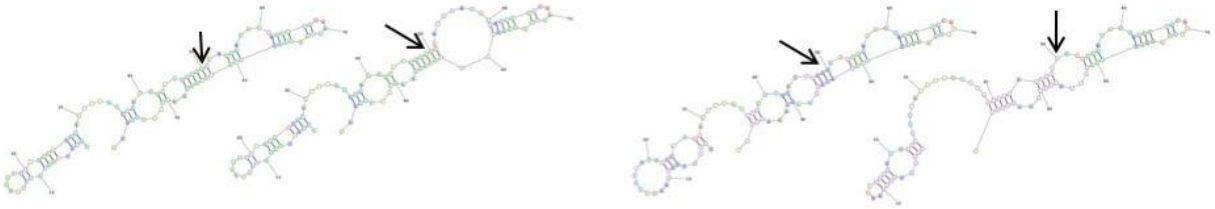

Figure S19: The observed rate constant for pseudouridinylation on short target 1 (ST1) is increased ~10-fold at elevated temperature. A. Observed rate constants for pseudouridinylation increase more than 10-fold as temperature increases, suggesting that increased conformational flexibility of the RNA structure allows more rapid access of PUS7. B. A set of stochastic structure predictions (32) demonstrating possible temperature-dependent changes in the structural environment of the target U in substrate sT1.

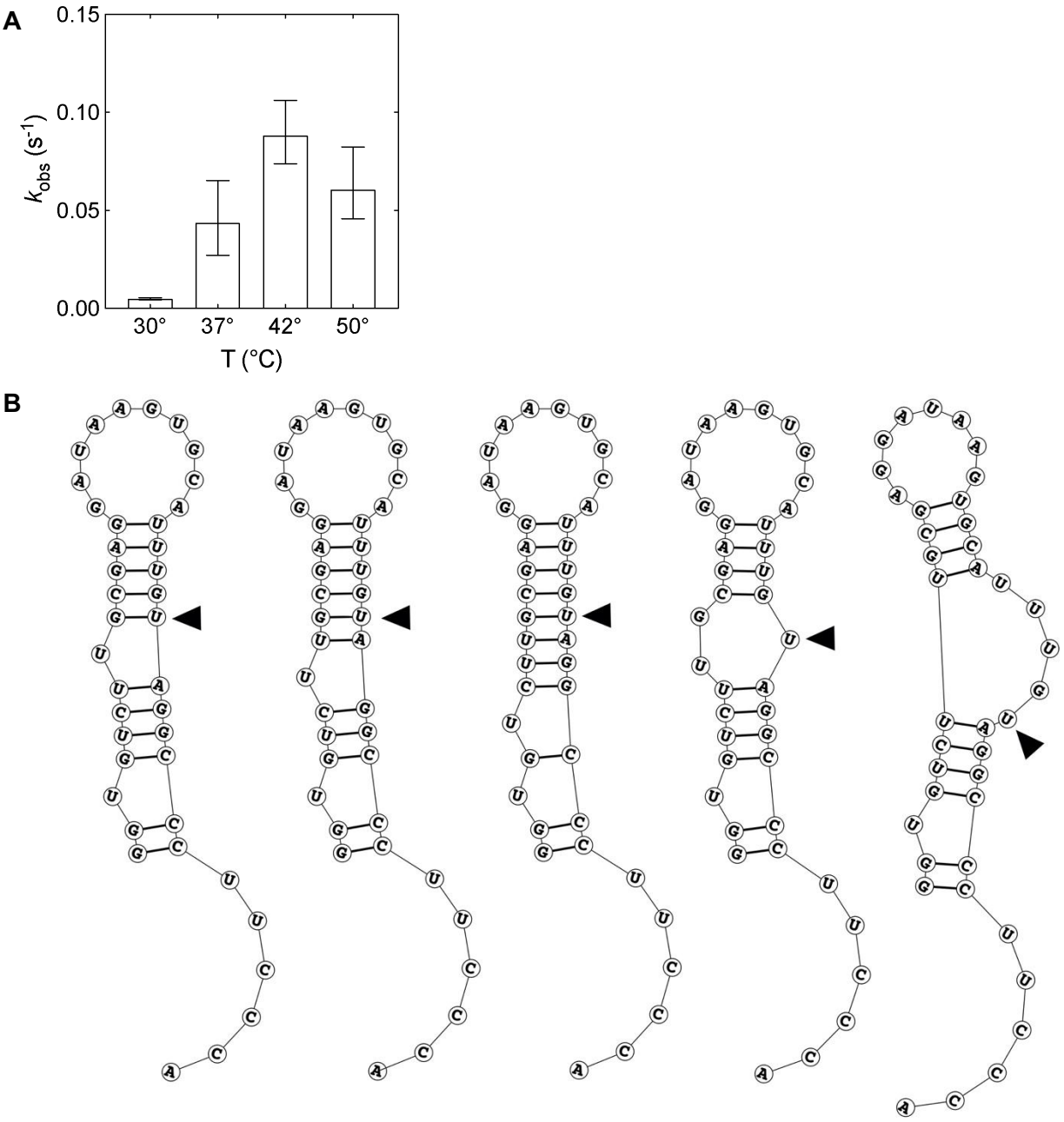

Figure S20: Modeled thermal stability of PUS7.
Using the chain length (N) of Pus 7, its stability was modeled as a function temperature range to find its maximum stability. Its maximum stability of about 65 kJ/mol is at approximately 22 ° C.

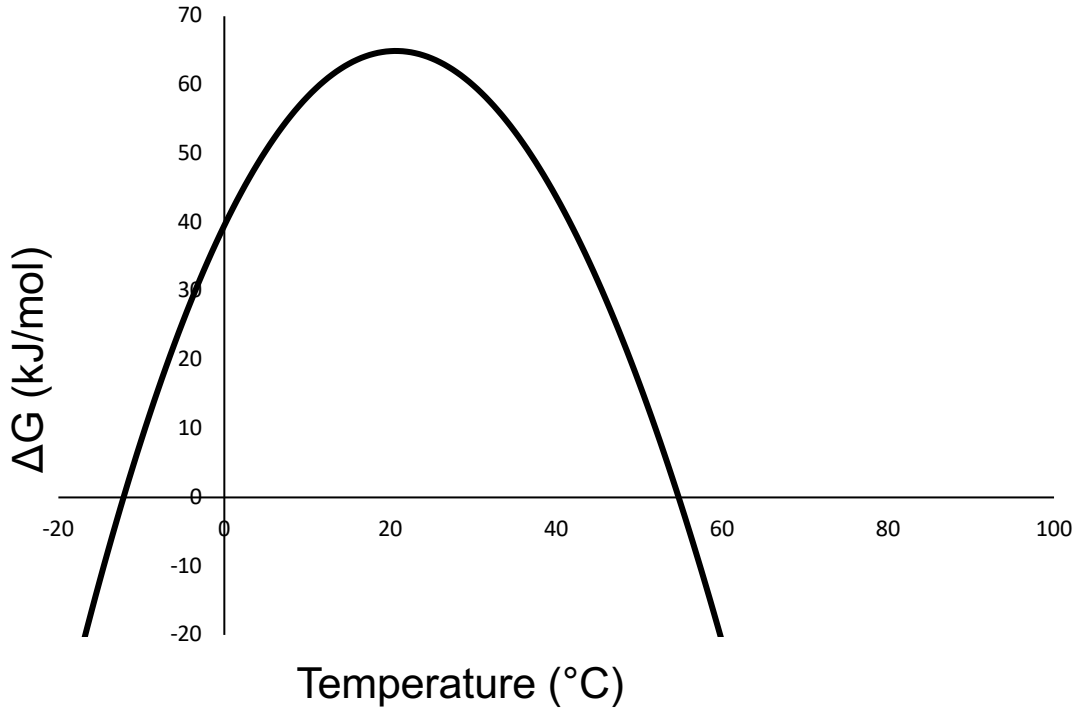

SUPPLEMENTAL APPENDIX TABLES

Table S1: Crystallographic parameters.

Table S1. X-Ray Crystallography Data Collection and Refinement Statistics

	Pus7
Data collection	
Beamline	APS, LSCAT 21-IDD
Wavelength (Å)	0.979
Temperature (K)	100
Resolution (Å)	48.27-3.20 (3.42-3.20)
Space group	*C*222
Cell dimensions (Å)	a = 117.9, b = 171.8, c = 105.3
Cell dimensions (°)	$\alpha = \beta = \gamma = 90$
Observed reflections	184,895 (31,045)
Unique reflections	18,019 (3,207)
R_{meas} (%)	17.8 (141.7)
R_{merge} (%)	17.8 (132.6)
$\langle I/\sigma \rangle$	9.5 (2.0)
CC(1/2)	0.996 (0.802)
Multiplicity	10.3 (9.7)
Completeness (%)	99.9 (100)
Overall *B* (Å^2) (Wilson plot)	121.9
Refinement	
Resolution range	46.32 - 3.20
Number of reflections (work/test set)	18017/881
R_{work}/R_{free} (%)	22.4/27.6
No. of non-H atoms	
Protein	9394
Water	14
Ligand	15
B-factors (Å^2)	
Protein	130.1
Water	88.7
Ligand	164.3
Rmsd deviations	
Bond lengths (Å)	0.0025
Bond angles (°)	1.21
Estimated coordinate error (Å); maximum likelihood based	0.4200
Cruickshank's DPI[1] (Å)	0.4688
Ramachandran plot	
Favored/allowed/outliers	87.7/12.1/0.2

MolProbity Score	1.63 (100^{th} percentile)
PDB	7MZV

Table S2: Impact of Pus7 mutations on CDC8 binding and modification

variant	k_{obs} (s^{-1}) [a,b]	k_{obs} defect (fold) [c]	$K_{D, app1}$ (nM) [d,e]
WT[e]	$9.9 \times 10^{-1} \pm 1.0 \times 10^{-1}$	1	76 ± 15
D256A[e]	no reaction		60 ± 16
K61A	$2.6 \times 10^{-2} \pm 0.1 \times 10^{-2}$	38 ± 6	400 ± 200
F67A	$4.6 \times 10^{-3} \pm 0.2 \times 10^{-3}$	210 ± 30	180 ± 40
E71A	$5.2 \times 10^{-3} \pm 0.3 \times 10^{-3}$	190 ± 30	210 ± 50
F307Y	$2.6 \times 10^{-3} \pm 0.1 \times 10^{-3}$	390 ± 60	378 ± 102
N305A	$4.0 \times 10^{-4} \pm \leq 1 \times 10^{-5}$	2,400 ± 300	230 ± 60
F307A	$1.3 \times 10^{-5} \pm \leq 1 \times 10^{-6}$	74,000 ± 9,000	344 ± 170
WT[f]	$8.4 \times 10^{-1} \pm 0.5 \times 10^{-1}$	1	n.d.[g]
H161A[f]	$6.9 \times 10^{-1} \pm 0.9 \times 10^{-1}$	1.2 ± 0.2	170 ± 40
ΔID1[f]	$3.8 \times 10^{-1} \pm 0.6 \times 10^{-1}$	2.2 ± 0.5	160 ± 40

[a] errors are standard error of the fit
[b] k_{obs} determined by fitting a curve of the form $y = 1 - e^{-k_{obs} \times t}$
[c] relative to WT at the same concentration on full-length cdc8 substrate
[d] K_D determined by curve fitting as described in Supplemental Appendix – Extended Methods
[e] All K_D values determined using D256A-double mutants, except for WT (no mutation), and the F307Y and D256A single mutants.
[f] Concentration of [Pus7] used to determine k_{obs} = 10 μM. All other reactions carried out with [Pus7] = 2 μM
[g] n.d., not determined

Table S3: Dissociation constants for Pus7 binding to various substrates.

substrate	variant	$K_{D,app1}$ (nM) [a,b]		
cdc8-A	WT	16	±	2
	D256A	57	±	4
cdc8-B	D256A	802	±	320
cdc8-C	WT	74	±	19
	D256A	131	±	13
sT1	D256A	34	±	4
	ΔID1-D256A	69	±	13
sT2	D256A	not analyzed – very weak		
	ΔID1-D256A	not analyzed – very, very weak		
$tRNA^{Asp}_{,GUC}$	D256A	16	±	1
	ΔID1-D256A	34	±	1

[a] errors are standard error of the fit
[b] K_D determined by curve fitting as described in the Extended Methods

Table S4: Observed rate constants for pseudouridinylation on different substrates.

substrate	variant	[PUS7] (μM)	k_{obs} (s^{-1}) [a,b]		
cdc8-A	WT	1	4.9×10^{-1}	±	0.5×10^{-1}
		5	9.3×10^{-1}	±	1.4×10^{-1}
		10	7.7×10^{-1}	±	0.8×10^{-1}
cdc8-B	WT	2	6.4×10^{-1}	±	1.0×10^{-1}
		10	7.8×10^{-1}	±	0.8×10^{-1}
cdc8-C	WT	2	8.9×10^{-1}	±	2.1×10^{-1}
		10	9.9×10^{-1}	±	1.4×10^{-1}
sT1	WT	10	5.1×10^{-3}	±	0.2×10^{-3}
	ΔID1	10	9.4×10^{-3}	±	0.7×10^{-3}
sT2	WT	10	2.4×10^{-4}	±	0.2×10^{-4}
$tRNA^{Asp,GUC}$	WT	10	9.1×10^{-3}	±	0.5×10^{-3}

[a] errors are standard error of the fit

[b] k_{obs} determined by fitting a curve of the form $fraction\ U \rightarrow = 1 - e^{-k_{obs} \times t}$

Table S5: RNAs used for biochemical assays.

substrate name	RNA sequence
cdc8-FL	GUCAAUCACGAUUGU**U**AGACGUUACUAAUAAGGGCAUUCAGGAAGU UGAAGCGCUUAUUUGG
CDC8-FL-NT	GUCAAUCACGAUUGCAGACGUUACUAAUAAGGGCAUUCAGGAAGU UGAAGCGCUUAUUUGG
CDC 8-A	GAUUGU**U**AGACGUUACUAAUAAGGGCAUUCAGGAAGUUGAAGCGCU UAUUUGG
CDC 8-A-NT	GAUUGCAGACGUUACUAAUAAGGGCAUUCAGGAAGUUGAAGCGCU UAUUUGG
CDC 8-B	GUCAAUCACGAUUGU**U**AGACGUUACU
CDC 8-B-NT	GUCAAUCACGAUUGCAGACGUUACU
CDC 8-C	GUCAAUCACGAUUGU**U**AGACGUUACUAAUAAGGGCGGAAGUGCGCU UAUUUGG
CDC 8-C-NT	GUCAAUCACGAUUGCAGACGUUACUAAUAAGGGCGGAAGUGCGCU UAUUUGG
ST1	GGUGUCUUGCGAGGAUAAGUGCAUUUGU**U**AGGCCCUUCCCA
SNT1	GGUGUCUUGCGAGGAUAAGUGCAUUUGCAGGCCCUUCCCA
ST2	GGGAUCUGU**U**AGCCCACCAA
SNT2	GGGAUCUGCAGCCCACCAA
tRNA^{Asp,GUC}	GCCGUGAUAG**U**UUAAUGGUCAGAAUGGGCGCUUGUCGCGUGCCA GAUCGGGGUUCAAUUCCCCGUCGCGGCGCCA
tRNA^{Asp,GUC}-NT	GCCGUGAUAGCUUAAUGGUCAGAAUGGGGCUUGUCGCGUGCCAG AUCGGGGUUCAAUUCCCCGUCGCGGCGCCA
CLAP-CDC8	GGCUAUUGGAUAAAGAGAUAAGGAAAGGCGAUGAGUCAAUCACGA UUGUAGACGUUACUAAUAAGGGCAUUCAGGAAGUUGAAGCGCUUA UUUGGCAAAUCGUUGAGCCUGUUUUGAGUACGCAUAU

SUPPLEMENTAL APPENDIX REFERENCES

1. McCoy AJ*, et al.* (2007) Phaser crystallographic software. *J Appl Crystallogr* 40(Pt 4):658-674.
2. Terwilliger TC*, et al.* (2009) Decision-making in structure solution using Bayesian estimates of map quality: the PHENIX AutoSol wizard. *Acta Crystallogr D Biol Crystallogr* 65(Pt 6):582-601.
3. Potterton L*, et al.* (2018) CCP4i2: the new graphical user interface to the CCP4 program suite. *Acta Crystallogr D Struct Biol* 74(Pt 2):68-84.
4. Emsley P, Lohkamp B, Scott WG, & Cowtan K (2010) Features and development of Coot. *Acta Crystallogr D Biol Crystallogr* 66(Pt 4):486-501.
5. Williams CJ*, et al.* (2018) MolProbity: More and better reference data for improved all-atom structure validation. *Protein Sci* 27(1):293-315.
6. Anonymous (The PyMOL Molecular Graphics System (Schrödinger, LLC).
7. Milligan JF, Groebe DR, Witherell GW, & Uhlenbeck OC (1987) Oligoribonucleotide synthesis using T7 RNA polymerase and synthetic DNA templates. *Nucleic Acids Res* 15(21):8783-8798.
8. Wright JR, Keffer-Wilkes LC, Dobing SR, & Kothe U (2011) Pre-steady-state kinetic analysis of the three Escherichia coli pseudouridine synthases TruB, TruA, and RluA reveals uniformly slow catalysis. *RNA* 17(12):2074-2084.
9. Kumar S, Stecher G, Li M, Knyaz C, & Tamura K (2018) MEGA X: Molecular Evolutionary Genetics Analysis across Computing Platforms. *Mol Biol Evol* 35(6):1547-1549.
10. Le SQ & Gascuel O (2008) An improved general amino acid replacement matrix. *Mol Biol Evol* 25(7):1307-1320.
11. Felsenstein J (1985) Confidence Limits on Phylogenies: An Approach Using the Bootstrap. *Evolution* 39(4):783-791.
12. Blanchet S*, et al.* (2018) Deciphering the reading of the genetic code by near-cognate tRNA. *Proc Natl Acad Sci U S A* 115(12):3018-3023.
13. Chou HJ, Donnard E, Gustafsson HT, Garber M, & Rando OJ (2017) Transcriptome-wide Analysis of Roles for tRNA Modifications in Translational Regulation. *Mol Cell* 68(5):978-992 e974.
14. Martin M (2011) Cutadapt removes adapter sequences from high-throughput sequencing reads. *EMBnet.journal* 17(1).
15. Tardu M, Jones JD, Kennedy RT, Lin Q, & Koutmou KS (2019) Identification and quantification of modified nucleosides in Saccharomyces cerevisiae mRNAs. *ACS Chem Biol* 14(7):1403-1409.
16. Langmead B & Salzberg SL (2012) Fast gapped-read alignment with Bowtie 2. *Nat Methods* 9(4):357-359.
17. Kim D*, et al.* (2013) TopHat2: accurate alignment of transcriptomes in the presence of insertions, deletions and gene fusions. *Genome Biol* 14(4):R36.
18. Lauria F*, et al.* (2018) riboWaltz: Optimization of ribosome P-site positioning in ribosome profiling data. *PLoS Comput Biol* 14(8):e1006169.
19. Li H*, et al.* (2009) The Sequence Alignment/Map format and SAMtools. *Bioinformatics* 25(16):2078-2079.
20. Jurrus E*, et al.* (2018) Improvements to the APBS biomolecular solvation software suite. *Protein Sci* 27(1):112-128.
21. Hoang C & Ferre-D'Amare AR (2004) Crystal structure of the highly divergent pseudouridine synthase TruD reveals a circular permutation of a conserved fold. *RNA* 10(7):1026-1033.

22. Dong A, Zeng, H., Walker, J.R., Bountra, C., Arrowsmith, C.H., Edwards, A.M., BROWN, P.J., WU, H., Structural Genomics Consortium (SGC) (2016) Crystal Structure of Human Pseudouridylate Synthase 7. (Protein Data Bank).
23. Carlile TM*, et al.* (2014) Pseudouridine profiling reveals regulated mRNA pseudouridylation in yeast and human cells. *Nature* 515(7525):143-146.
24. Schwartz S*, et al.* (2014) Transcriptome-wide mapping reveals widespread dynamic-regulated pseudouridylation of ncRNA and mRNA. *Cell* 159(1):148-162.
25. Zhang W, *et al*. (2019) Sensitive and quantitative probing of pseudouridine modifications in mRNA and long noncoding RNA. *RNA* 25(9):1218-1225.
26. Myers, J. K.; Pace, C. N.; Scholtz, J. M. Denaturant m Values and Heat Capacity Changes: Relation to Changes in Accessible Surface Areas of Protein Unfolding. Protein Science : A Publication of the Protein Society 1995, 4 (10), 2138. https://doi.org/10.1002/pro.5560041020.
27. Ghosh, K.; Dill, K. A. Computing Protein Stabilities from Their Chain Lengths. PNAS 2009, 106 (26), 10649–10654. https://doi.org/10.1073/pnas.0903995106.
28. Sawle, L.; Ghosh, K. How Do Thermophilic Proteins and Proteomes Withstand High Temperature? Biophys J 2011, 101 (1), 217–227. https://doi.org/10.1016/j.bpj.2011.05.059.
29. Watson, M. D.; Monroe, J.; Raleigh, D. P. Size-Dependent Relationships between Protein Stability and Thermal Unfolding Temperature Have Important Implications for Analysis of Protein Energetics and High-Throughput Assays of Protein–Ligand Interactions. J. Phys. Chem. B 2018, 122 (21), 5278–5285. https://doi.org/10.1021/acs.jpcb.7b05684.
30. Rees, D. C.; Robertson, A. D. Some Thermodynamic Implications for the Thermostability of Proteins. Protein Sci 2001, 10 (6), 1187–1194.
31. Robertson, A. D.; Murphy, K. P. Protein Structure and the Energetics of Protein Stability. Chem. Rev. 1997, 97 (5), 1251–1268. https://doi.org/10.1021/cr960383c.
32. Harmanci, A. O., Sharma, G., & Mathews, D. H. (2009). Stochastic sampling of the RNA structural alignment space. Nucleic Acids Research. 37, 4063-4075.